SPHERE DRAG IN THE FREE-MOLECULAR AND TRANSITIONAL FLOW REGIMES

David L. Whitfield and William B. Stephenson
ARO, Inc.

April 1970

AEROSPACE ENVIRONMENTAL FACILITY
ARNOLD ENGINEERING DEVELOPMENT CENTER
AIR FORCE SYSTEMS COMMAND
ARNOLD AIR FORCE STATION, TENNESSEE

NOTICES

When U. S. Government drawings specifications, or other data are used for any purpose other than a definitely related Government procurement operation, the Government thereby incurs no responsibility nor any obligation whatsoever, and the fact that the Government may have formulated, furnished, or in any way supplied the said drawings, specifications, or other data, is not to be regarded by implication or otherwise, or in any manner licensing the holder or any other person or corporation, or conveying any rights or permission to manufacture, use, or sell any patented invention that may in any way be related thereto.

Qualified users may obtain copies of this report from the Defense Documentation Center.

References to named commercial products in this report are not to be considered in any sense as an endorsement of the product by the United States Air Force or the Government.

SPHERE DRAG IN THE FREE-MOLECULAR AND TRANSITIONAL FLOW REGIMES

David L. Whitfield and William B. Stephenson
ARO, Inc.

FOREWORD

This work was sponsored by the Air Force Cambridge Research Laboratories (AFCRL) (CRMP), Bedford, Massachusetts, under Program Element 62101F, Project 6690, Task 669002.

The results presented were obtained by ARO, Inc. (a subsidiary of Sverdrup & Parcel and Associates, Inc.), contract operator of the Arnold Engineering Development Center (AEDC), Air Force Systems Command (AFSC), Arnold Air Force Station, Tennessee, under Contract F40600-69-C-0001. This work was conducted from April 14 to September 26, 1969, under ARO Project No. SB0913. The manuscript was submitted for publication on January 2, 1970.

The authors wish to acknowledge the assistance of two cooperative engineering students in performing this work, Jack L. Womack (University of Tennessee) and Norman O. Speakman (Auburn University).

This technical report has been reviewed and is approved.

Robert T. Otto
Major, USAF
AF Representative, AEF
Directorate of Test

Roy R. Croy, Jr.
Colonel, USAF
Director of Test

ABSTRACT

Results are presented of sphere drag measurements made in the free-molecular and transitional flow regimes. The drag data were obtained using a drag balance and the free-flight technique. Conditions for which measurements were made are within the ranges $1 < Kn_\infty < 32$, $2.9 < M_\infty < 11.2$, $0.8 < T_w/T_\infty < 16.0$, and $2.5 < S_w < 3.2$. An analysis of the drag on a sphere in rarefied flow is also presented, and the results are compared with experimental data and other theories. The analytical results well predict the trend of the experimental data in the transition regime and remain valid at Knudsen numbers for which previous theories are not applicable.

CONTENTS

APPENDIXES

I. ILLUSTRATIONS

Figure

Page

NOMENCLATURE

A	Cross-sectional area of sphere, πr^2
C_D	Drag coefficient, defined by Eq. (1)
C_p	Specific heat of gas at constant pressure
C_v	Specific heat of gas at constant volume
$c_1, c_2, c_3,$	Constants, Eq. (2)
D	Drag
d	Sphere diameter
erf(x)	Error function, $2/\sqrt{\pi} \int_0^x e^{-t^2}\, dt$
H	Local total enthalpy
Kn	Knudsen number
M	Mach number
m	Mass of sphere
N	Number flux of molecules
$\bar{N}$	Number of molecules per unit time
n	Number density of molecules
P	Pressure
P_o'	Total pressure immediately downstream of a normal shock
P_p	Measured pitot pressure
q	Dynamic pressure, $\rho U^2/2$
R	Gas constant

Re	Reynolds number based on sphere diameter, also pitot probe diameter in Fig. 4
Re_{o,r^*}	Nozzle reservoir Reynolds number, $\rho_o\sqrt{2H_o}\ r^*/\mu_o$
Re_w	$\rho_\infty U_\infty d/\mu_w$
Re_∞	$\rho_\infty U_\infty d/\mu_\infty$
r	Radius of sphere
r^*	Nozzle throat radius
S	Speed ratio, $U/(2RT)^{1/2}$
S_w	$U_\infty/(2RT_w)^{1/2}$
S_∞	$U_\infty/(2RT_\infty)^{1/2}$
T	Temperature
t	Time
U	Velocity
v	Velocity of molecules emitted from the sphere surface
x	Axial coordinate
γ	Ratio of specific heats, C_p/C_v
λ	Mean free path, $(\pi/2RT)^{1/2}\ \mu/\rho$
μ	Viscosity
ρ	Gas mass density
σ	Effective molecular diameter

SUBSCRIPTS

2	Condition immediately downstream of a normal shock
℄	Nozzle centerline
c	Collision molecules

E	Nozzle exit
fm	Free-molecular value
i	Incident molecules
o	Reservoir (total condition)
s	Surviving molecules
w	Sphere wall condition
∞	Free-stream condition

SECTION I
INTRODUCTION

Investigations of atmospheric winds, density, pressure, and temperature using spherical satellites and falling balloons (Ref. 1) have stimulated interest in sphere drag from subsonic to hypersonic flow and from the continuum to the free-molecular regime. Besides the dependency of drag on the Mach number, or speed ratio, drag in the free-molecular and transitional flow regimes depends significantly on the sphere wall and free-stream gas temperatures. Also, there is the possibility that various materials will have different accommodation coefficients at satellite velocities and thereby influence the drag. An example of a body which may have all of these factors influencing the drag simultaneously would be a satellite designed with surface materials of different emissivities to provide thermal control. An accurate measurement of the drag of such a body is very difficult because (1) in order to simulate high Knudsen number ($Kn_\infty = \lambda_\infty/d$) flow in present low density test facilities, the model must be relatively small and this makes actual simulation of the model difficult, and (2) the actual surface condition of the materials is difficult to reproduce even if the same materials and paints are used, because of condensed gases, etc., on the surface of the model which may not be present in space. The effect of wall temperature on drag can be measured in wind tunnel experiments, and the effect of surface condition on drag is usually not as large and can be investigated better using a molecular beam. Therefore, the effect of surface condition on drag will not be discussed other than the presentation of data taken using a sphere with a black and then a gold surface.

The purpose of this report is to present the results of sphere drag measurements made in the free-molecular and transitional flow regimes. A theoretical analysis of the drag on a sphere in the transition regime is also presented, and the theoretical and experimental results are compared. This analysis predicts the free-molecular drag value as $Kn_\infty \to \infty$ and the Newtonian drag value as $Kn_\infty \to 0$. The present results are compared with other analytical and experimental investigations (Refs. 2 through 9).

SECTION II
EXPERIMENTAL PROCEDURE

The experimental data were taken in the Aerospace Research Chamber (ARC) (8V) of the Aerospace Environmental Facility (AEF) at AEDC. This chamber is 10 ft in diameter, 20 ft in length, and uses cryogenic surfaces to pump the gas from the wind tunnel nozzle. The principal pumping capacity of the ARC (8V) chamber was provided by 620 ft^2 of 77°K liquid-nitrogen cryosurfaces and 240 ft^2 of 15 to 20°K gaseous-helium cryosurfaces. A total of 4-kw gaseous-helium refrigeration capacity was used. This arrangement permitted the continuous pumping of nitrogen or argon at a mass flow rate of 10 gm/sec at a chamber pressure of about 10^{-5} mm Hg. The pumping requirements for this test were less than 10 gm/sec.

Drag measurements were made using a balance and a free-flight technique. The design, calibration, and operation of the equipment and instrumentation necessary for these two methods of measuring drag are discussed in detail in Ref. 10. The data reduction techniques are discussed here.

2.1 WIND TUNNEL NOZZLES

Two low density nozzles, designated as the Mach number 3 (M3) and Mach number 6 (M6) nozzles, were used to provide the flow conditions. The wall cooling on the M6 nozzle was recently modified by replacing the aluminum tubing through which liquid nitrogen was forced, by a complete liquid-nitrogen jacket similar to the M3 nozzle. The result was to produce a constant 89°K wall temperature which was a 100°K decrease in wall temperature at the nozzle exit. This reduction in wall temperature reduced the boundary-layer growth on the nozzle wall and also improved the repeatability of the flow in the nozzle since the wall temperature remained constant with time. Some results on the flow conditions in the M3 nozzle using nitrogen or argon as the test gas are given in Ref. 11. Boundary-layer profiles and axial-flow conditions for the M3 nozzle, and more results on the flow conditions in the M3 and M6 nozzles, for nitrogen only, are given in Refs. 12 and 13. A summary of the operating ranges of these nozzles is given in Fig. 1 (Appendix I).

2.2 NOZZLE CALIBRATION

The total pressure, P_o, was obtained using an MKS Baratron ® (variable capacitance transducer), which measured the average of the pressure at two locations in the reservoir as shown in Fig. 2. The total temperature, T_o, was measured using a total temperature probe located on the centerline of the reservoir (Fig. 2). The flow was calibrated using a 1-in.-diam, 10-deg internally chamfered pitot probe. A Baratron was used to measure the pitot pressure. The pitot probe was mounted on a scanner mechanism as shown in Fig. 2. The movement of the scanner, which was in the plane of the figure, permitted the measurement of pitot pressures from 5 in. inside to 20 in. downstream of the nozzle exit planes and from 5 in. below to 20 in. above the nozzle centerlines. The vertical movement was sufficient to traverse the exit radii of the two nozzles.

For the rarefied flow conditions of interest, the viscous corrections to the pitot pressure measurements were significant. The magnitude of this effect on Mach number and dynamic pressure, q_∞, is illustrated in Fig. 3 for the M6 nozzle. Since the drag coefficient is inversely proportional to q_∞, it is obvious from Fig. 3 that serious error is introduced if the viscous correction is not known accurately. The viscous correction data used to correct the pitot pressure measurements were obtained in a previous test program, and these data are given in Fig. 4 with data from other sources (Refs. 14 through 17).

A problem associated with low density wind tunnel testing is that of boundary-layer merging, i.e., the boundary layer completely filling the nozzle. It has been previously assumed that merging in the M6 nozzle occurred at the point of minimum

Mach number (Fig. 3).This assumption has since been found to be invalid for the following reason. It was observed that an abrupt increase in the drag coefficient occurred at values of Kn_∞ where the drag coefficient should be free molecular or at least be asymptotically approaching the free-molecular limit. In order to explain the unexpected increase in C_D, an investigation was made to determine whether or not the flow was merged, because if it was, the pitot pressure measurements would be incorrect and the free-stream properties, q_∞, T_∞, etc., calculated using P_o, T_o, and P_o', would also be incorrect. The problem of merged flow was investigated using the fully viscous slender-channel program developed by Rae (Ref. 18). It was found from the numerical solutions that a significant decrease in the local total enthalpy, H, occurred at the M6 nozzle exit centerline at about the same point, i.e., value of P_o for T_o = constant, at which the increase in C_D occurred (Fig. 5). The decrease in $H_{Q_l,E}$ indicated the flow was not isentropic, and hence the q_∞ used to determine C_D for $P_o < 1$ mm Hg was incorrect. The value of nozzle reservoir Reynolds number, Re_{o,r^*}, at which merging occurred for this value of the nozzle wall to reservoir temperature ratio (which was 0.11), was $Re_{o,r^*} = 900$. The throat radius for this nozzle was $r^* = 1.54$ in. It is interesting to note that merging actually occurred for the conditions in Fig. 3 at $P_o \approx 1$ mm Hg, which was a significantly larger value of P_o than the value at which the minimum Mach number occurred. Numerical solutions were also obtained for the flow in the M3 nozzle; however, data are presented only for isentropic flow conditions.

2.3 DATA REDUCTION

2.3.1 Drag Balance

Data reduction of the forces measured using the drag balance was straightforward. After force measurements were made on the sphere mounted on the sting at various flow conditions, the sphere was removed, and a second sphere, independently supported, was positioned slightly upstream of the sting (Fig. 6). The tare forces on the sting were measured using this arrangement for the same range of flow conditions for which total force measurements were made. An example of the tare force and total drag force measurements is given in Fig. 6. For this 0.25-in.-diam sphere, the tare force was from 15 to 20 percent of the total drag force. If the sphere size was reduced, the percent of total force which was attributable to tare increased. The difference between tare and total force measurements is the sphere drag, D. The drag coefficient, C_D, was obtained from the definition

$$C_D = \frac{D}{1/2\,\rho_\infty U_\infty^2 A} = \frac{D}{q_\infty A} \tag{1}$$

A second sphere, identical to the one used on the balance sting to measure the drag, was used to determine the sphere wall temperature. This second sphere was supported by the leads to a thermocouple which was used to measure the sphere temperature. It was attached to the same support as the balance and was simultaneously subjected to the same flow conditions as the sphere mounted on the balance sting. It was assumed that the temperature of the sphere was uniform, and therefore the measured temperature was taken as the sphere wall temperature.

2.3.2 Free Flight

Free-flight drag data were obtained from photographs of the trajectories of spheres (Fig. 7) which were dropped through the nozzle test section. The photographs were multiple exposures of spheres illuminated at constant time intervals by a strobe light operating at the rate of 120 flashes/sec. From one to three aluminum and/or magnesium spheres were dropped simultaneously. The spheres were initially located in the drop mechanism a minimum of ten diameters apart in a plane perpendicular to the plane of the photograph in Fig. 7. Immediately after the spheres were dropped, the minimum separation distance increased, and it was assumed that no interaction among the spheres occurred. Sphere diameters of 1/32, 1/16, and 1/8 in. were used. The sphere wall temperatures were determined by measuring the temperature of the drop mechanism. The change in sphere temperature for the period of time required for the spheres to traverse the test section was negligible.

The drag force on a sphere was determined by applying Newton's second law of motion to the sphere in the direction of the free-stream velocity. The distance, x, which a constant mass body would move in a constant force field is a quadratic equation in time, t, i.e.,

$$x = c_1 t^2 + c_2 t + c_3 \tag{2}$$

Using Newton's law

$$D = m \frac{d}{dt}\left(\frac{dx}{dt}\right) \tag{3}$$

and substituting Eq. (2) into Eq. (3) and differentiating gives

$$D = 2mc_1 \tag{4}$$

where m is the mass of the sphere. Therefore, if c_1 can be determined, the drag can be calculated. The constant c_1 was determined by fitting a second-order polynomial through the data of a plot of x versus t (Fig. 8). The value of x for each t was determined by measuring the axial displacement of the sphere from point to point in Fig. 7 at constant (known) intervals of time. These measurements were made from the photographic negatives using a film reader.

SECTION III
TRANSITION DRAG ANALYSIS

A simple analysis is presented for the drag of spheres in the transitional flow regime. The mathematical model is based on the following four assumptions: (1) The flow Mach number is sufficiently high that the number flux of molecules which has a chance of colliding with the sphere is given by $N_\infty = n_\infty U_\infty$, (2) all molecules are emitted normal to the sphere surface, (3) each emitted molecule experiences only one collision with an oncoming free-stream molecule, after which neither molecule is considered, and (4) all collisions occur at a distance λ_w from the sphere surface (Fig. 9).

There are certain restrictions and conditions which need to be considered because of the basic assumptions. The first assumption requires that the random molecular velocity be less than the mean flow velocity. Physically this means that the molecules tend to move in straight lines parallel to the mean flow direction, and therefore, the net number which cross the boundary of the imaginary cylinder swept out by the sphere per unit time, i.e., $\pi r^2 U_\infty$, is negligible. This is not a particularly stringent assumption, as indicated by the results given in Fig. 10 for the incident flux in free-molecular flow (see Ref. 19 for a derivation of the incident flux). From Fig. 10 the approximation $N_i \approx N_\infty = n_\infty U_\infty$ is good for $S_\infty > 1$ or $(2RT_\infty)^{1/2} < U_\infty$.

The second assumption permits one to neglect the distribution function of the molecules emitted from the sphere surface, and it is justified only by the final results.

The third and fourth assumptions, together, imply that the sphere is in free-molecular flow with respect to molecules which survive the collision surface (Fig. 9) since there are no collisions between free-stream and emitted molecules in the region between the collision surface and the sphere. Therefore, by determining the number flux of surviving molecules, $n_s U_\infty$, the drag on a sphere can be determined from

$$\frac{D}{D_{fm}} = \frac{C_D}{C_{D_{fm}}} = \frac{n_s}{n_\infty} \tag{5}$$

since the drag on the sphere is the same as the free-molecular drag with a free-stream number density of n_s. That is, for the same free-stream and sphere wall conditions, the drag is proportional to the free-stream number density, or, for the case of the surviving molecules, to the effective free-stream number density, n_s.

Before solving for $n_s U_\infty$, it is interesting to note an error introduced by considering the ratio $C_D/C_{D_{fm}}$ in Eq. (5). It was assumed in writing Eq. (5) that the free-stream conditions of the surviving molecules, other than number density, did not change, and also that the sphere wall conditions did not change. The assumption of constant free-stream conditions is valid because of the four basic assumptions, but the one concerning the wall conditions is not. This is because fewer molecules are available to transfer heat between the gas and the sphere because of the "shielding" effect produced by the collisions, and therefore, T_w is not the same for the shielded and unshielded sphere. However, for a diffusely reflecting wall, which was the model assumed in calculating $C_{D_{fm}}$ for the experimental data, the effect of T_w decreases as S_∞ increases (Fig. 11), and it is assumed that the effect of the difference between wall temperatures on C_D is negligible. Of course for a specularly reflecting wall, C_D is independent of T_w, and no error is introduced.

In the solution for $n_s U_\infty$ the mean distance between collisions of emitted molecules with oncoming molecules, λ_w, will be taken as a function of ψ as given by (Refs. 2 and 20)..

$$\lambda_w = \frac{v_w}{\pi\sigma^2 n_\infty \left[(U_\infty + v_w \cos\psi)^2 + (v_w \sin\psi)^2\right]^{1/2}} \tag{6}$$

In terms of the mean free path of the molecules in the free stream. $\lambda_\infty = 1/(\sqrt{2}\pi\sigma^2 n_\infty)$, Eq. (6) can be written

$$\frac{\lambda_w}{\lambda_\infty} = \frac{\sqrt{2}\, v_w}{[U_\infty^2 + 2U_\infty v_w \cos\psi + v_w^2]^{1/2}} \tag{7}$$

Since the number flux which has a chance of colliding with the sphere is $n_\infty U_\infty$, then only those collisions which occur at the "effective collision surface" (which is that part of the collision surface within the cylindrical volume swept out by the sphere, Fig. 9) will affect the surviving number flux which reaches the sphere. The number of molecules per unit time which survive, $\bar{N}_s$, can be expressed as

$$\bar{N}_s = \bar{N}_\infty - \bar{N}_c \tag{8}$$

where

$$\bar{N}_\infty = n_\infty U_\infty \pi r^2 \tag{9}$$

is the number of free-stream molecules per unit time which would collide with the sphere if no collisions between emitted and free-stream molecules occurred, and $\bar{N}_c$ is the number of molecules per unit time which are emitted toward the effective collision surface and hence suffer collisions with free-stream molecules. Therefore, $\bar{N}_c$ is the number per unit time which are removed from $\bar{N}_\infty$. Since the molecules were assumed to be emitted normal to the sphere surface, the number of molecules emitted from the sphere surface within the angle θ is equal to $\bar{N}_c$ as expressed by

$$\bar{N}_c = n_s U_\infty A_P = n_s U_\infty \int_0^\theta 2\pi r^2 \sin\psi \cos\psi \, d\psi \tag{10}$$

where n_s is the number density behind the collision surface, and the integral, A_P, is the projected surface area of the sphere within θ (Fig. 9). Integrating Eq. (10) gives

$$\bar{N}_c = n_s U_\infty \pi r^2 \sin^2\theta \tag{11}$$

Expressing $\bar{N}_s$ as

$$\bar{N}_s = n_s U_\infty \pi r^2 \tag{12}$$

which is the total number per unit time which survive to collide with the sphere, and then substituting Eqs. (9), (11), and (12) into Eq. (8) gives

$$n_s U_\infty = n_\infty U_\infty - n_s U_\infty \sin^2\theta \tag{13}$$

Solving for n_s/n_∞ one has

$$\frac{n_s}{n_\infty} = \frac{1}{1 + \sin^2\theta} \tag{14}$$

Substituting Eq. (14) into Eq. (5) and using A_P/A for $\sin^2\theta$ (Eqs. (10) and (11)) gives

$$\frac{C_D}{C_{D_{fm}}} = \frac{1}{1 + \sin^2\theta} = \frac{1}{1 + \frac{A_P}{A}} \tag{15}$$

The angle θ depends on λ_w since θ is the angle at which the distance between the collision surface and sphere surface in the θ direction is equal to λ_w (Fig. 9). From the geometry in Fig. 9 one can write

$$\sin\theta = \frac{r}{r + \lambda_w|_{\psi=\theta}} \tag{16}$$

Substituting Eq. (16) into Eq. (15) gives

$$\frac{C_D}{C_{D_{fm}}} = \frac{1}{1 + \dfrac{1}{\left[1 + \dfrac{\lambda_w}{r}|_{\psi=\theta}\right]^2}} \tag{17}$$

Using Eq. (7) for λ_w, the term λ_w/r becomes

$$\frac{\lambda_w\,(Kn_\infty, S_w, \theta)}{r} = \frac{2\sqrt{2}\,Kn_\infty}{\left[\left(\dfrac{4S_w}{3\sqrt{\pi}}\right)^2 + 2\left(\dfrac{4S_w}{3\sqrt{\pi}}\right)\cos\theta + 1\right]^{1/2}} \tag{18}$$

where $Kn_\infty = \lambda_\infty/d$, $S_w = U_\infty/(2RT_w)^{1/2}$, and $v_w = (9\pi RT_w/8)^{1/2}$ (Ref. 5). Substituting Eq. (18) into Eq. (17) gives for the drag coefficient

$$\frac{C_D}{C_{D_{fm}}} = \frac{1}{1 + \left\{\dfrac{1}{1 - \dfrac{2\sqrt{2}\,Kn_\infty}{\left[\left(\dfrac{4S_w}{3\sqrt{\pi}}\right)^2 - 2\left(\dfrac{4S_w}{3\sqrt{\pi}}\right)\cos\theta + 1\right]^{1/2}}}\right\}^2} \tag{19}$$

An expression for θ used in Eq. (19) can be obtained by substituting Eq. (18) into Eq. (16) to get

$$\sin\theta = \frac{1}{1 + \dfrac{2\sqrt{2}\,Kn_\infty}{\left[\left(\dfrac{4S_w}{3\sqrt{\pi}}\right)^2 + 2\left(\dfrac{4S_w}{3\sqrt{\pi}}\right)\cos\theta + 1\right]^{1/2}}} \tag{20}$$

Equation (20) is a transcendental equation which must be solved for θ for each value of Kn_∞ and S_w. The solution for θ which satisfies $0 < \theta < \pi/2$ (Fig. 9) was used in Eq. (19) to calculate $C_D/C_{D_{fm}}$ for each value of Kn_∞ and S_w.

SECTION IV
RESULTS AND DISCUSSION

4.1 ANALYTICAL

It is of interest to examine the limits of Eq. (19). In the limit $Kn_\infty \to \infty$ the result for the drag coefficient is $C_D/C_{D_{fm}} = 1$, which is, of course, expected. In the limit $Kn_\infty \to 0$ the result for the drag coefficient is $C_D/C_{D_{fm}} = 0.5$. This result can be reasoned physically by recalling that one of the assumptions was that only one collision between

emitted and free-stream molecules was considered. Therefore, when the mean free path $\lambda_\infty = 0$ (and hence $\lambda_w = 0$, see Eq. (18)), only one-half the molecules which have a chance of colliding with the sphere could actually collide, since each molecule at the sphere surface prevented another molecule from colliding with the surface. This result is the same as the result obtained from the Newtonian theory if $C_{D_{fm}}$ is based on specular reflection. Newtonian theory assumes that all the molecules directly upstream of the sphere hit the sphere but that they impart momentum because of the collision only, since they leave parallel to the surface. Whereas, in the present analysis, only one-half the molecules directly upstream of the sphere hit the sphere, but they impart momentum from both the collision and the reflection. This is the reason for a sensible result in the continuum limit.

Some results from Eq. (19) are given in Fig. 12 where θ was obtained from the solution to Eq. (20) for each value of Kn_∞ and S_w. Notice in Fig. 12 that $C_D/C_{D_{fm}}$ decreases as S_w increases. That is, for constant free-stream conditions, the collision surface approaches the sphere surface as S_w increases, because of decreasing T_w and hence decreasing λ_w, and consequently more shielding occurs, and the drag is reduced.

A simplification in the calculation of the drag coefficient is obtained if λ_w in Eq. (17) is taken as a function of Kn_∞ and S_w only, i.e., if θ in Eq. (18) is taken as constant. The effect of the θ term in Eq. (18) is shown in Fig. 13 to have relatively little effect on the value of λ_w, or Kn_w, for constant S_w. The assumption of constant θ in Eq. (18) eliminates the necessity of solving Eq. (20). The resulting drag coefficients as calculated using constant and variable λ_w are illustrated in Fig. 14 for $S_w = 1$. For small values of Kn_∞ the result with $\lambda_w(\theta = \pi/2)$ gives slightly better agreement with variable λ_w, whereas for large values of Kn_∞ the result with $\lambda_w(\theta = 0)$ gives better agreement. This result is expected since for small Kn_∞, $\theta \approx \pi/2$, and for large Kn_∞, $\theta \approx 0$ (Fig. 9). In general, for all Kn_∞, the result with λ_w ($\theta = 0$) gives better agreement with the result for variable λ_w (Fig. 14). It should be pointed out that the assumption of constant θ in Eq. (18) is justified only because λ_w is a weak function of θ and a strong function of Kn_∞ and S_w.

4.2 EXPERIMENTAL

4.2.1 Balance Data

Drag measurements were made using the balance in the M3 and M6 nozzle flows. The reservoir (total) temperature was 800°K, and the total pressure was varied between 0.1 and 5.0 mm Hg, depending on the nozzle used, to produce free-stream Knudsen numbers of $1 < Kn_\infty < 5$, based on a 0.25-in.-diam sphere.

The balance proved capable of measuring the change in sphere drag which was caused only by a changing wall temperature. The wall temperature of the 0.25-in.-diam sphere used to take the data in Fig. 15 varied between 253 and 314°K, and the free-stream gas static temperature, T_∞, varied between 74 and 62°K. Taking into account the appropriate S_∞ and T_w/T_∞ ratio in the calculation of $C_{D_{fm}}$, the drag data normalized by $C_{D_{fm}}$ have less deviation than the C_D data as shown in Fig. 15. The assumption used for the calculation of $C_{D_{fm}}$ was that the molecules were completely accommodated and reflected diffusely from the sphere surface (Fig. 11).

The balance drag data are shown in Fig. 16 by the closed symbols. The data taken in the M6 nozzle, i.e., $7.0 < M_\infty < 7.7$, have less than 2-percent scatter, and the data taken in the M3 nozzle have slightly more scatter. The difference, if any, in the drag between the two spheres with painted surfaces, one coated with a flatblack lacquer paint of high emissivity, which was used for thermal control on satellites, and the other coated with gold, could not be detected.

The drag coefficients and flow conditions for the balance data are tabulated in Table I (Appendix II).

4.2.2 Free-Flight Data

The free-flight drag data using nitrogen and argon as the test gas are also given in Fig. 16. The scatter in the free-flight data is obviously much worse than the scatter in the balance data. There are several possible explanations for the scatter in the free-flight data. Among them are: (1) The spheres were dropped through the test section with initial direction normal to the free stream rather than directly upstream as is usually done in free-flight measurements, and therefore, small axial displacements of the spheres were obtained because of the low free-stream dynamic pressure and the requirement that the spheres be at least 1/32 in. in diameter in order to be photographed, (2) the strobe light used was limited to 120 flashes/sec, and this restricted the number of exposures of the spheres which could be made during the free fall, (3) error in reading the sphere trajectories from the photograph negatives, (4) large distance, 9 ft, from the camera and strobe light to the spheres, and (5) the portion of the test section through which the spheres fell had an axial Mach number gradient of about 0.05/in., and the flow conditions used to reduce the sphere data corresponded to that point in the flow where the spheres crossed the nozzle axis (the maximum axial displacement of the spheres was about 6 in.). Suggestions to eliminate or reduce the magnitude of these effects are given in Ref. 10.

The drag coefficients and flow conditions for the free-flight data are tabulated in Table I.

4.3 ANALYTICAL AND EXPERIMENTAL COMPARISONS

Compared with the balance and free-flight drag data in Fig. 16 is the analytical result given by Eq. (19) for $S_w = 2.7$, which is a mean value of the wall speed ratio for these data. From this comparison the analysis appears to provide a reasonable prediction of the drag in the near free-molecular regime. Certainly the agreement between theory and experiment is good, considering the simple mathematical model used to analyze the drag in the transition regime.

In order to determine the qualitative trend of the analysis throughout the transitional flow regime, Eq. (19) is compared with drag data from various sources in Fig. 17 for two values of S_w which essentially bound the experimental data. As can be seen in Fig. 17, the trend of the experimental data in the transition regime is relatively well predicted. However, the experimental data of Fig. 17 do not always vary with S_w as the

analytical results predict. Therefore, the solution for $S_w = 1$ was taken to compare with some data in Fig. 18 which have little scatter. It was found that the solution for $S_w = 1$ provided the best agreement with the bulk of the experimental data. Furthermore, if λ_w is taken as constant with respect to θ, then the curve in Fig. 18 can be rather accurately approximated by

$$\frac{C_D}{C_{D_{fm}}} = \frac{1}{1 + \left[\frac{1}{1 + 1.615\ Kn_\infty}\right]^2} \tag{21}$$

which, in terms of M_∞, Re_∞, and γ, can be written as

$$\frac{C_D}{C_{D_{fm}}} = \frac{1}{1 + \left[\frac{1}{1 + \frac{2.02\sqrt{\gamma}\ M_\infty}{Re_\infty}}\right]^2} \tag{22}$$

A comparison is made in Fig. 19 of the present result with the theories of Baker and Charwat (Ref. 2), Rose (Ref. 3), and Willis (Ref. 4) and some experimental data for S_w near 1.6. The theories of Rose and Willis depend on S_∞ and are calculated only for the conditions of Sims' data (Ref. 7). They should not be expected to compare with the other data, although the conditions of the data of Ref. 6 are close to those of Sims' data (the different test gases used should be noted, however). The present result and the theory of Baker and Charwat do not depend on S_∞ and therefore are applicable to all the data in Fig. 19. As can be seen in Fig. 19, the theory of Willis and the present result well predict these drag data in the near free-molecular regime. Also, the present result continues to predict these drag data at Knudsen numbers below which the existing theories shown in Fig. 19 are not applicable.

SECTION V
CONCLUSIONS

Sphere drag measurements have been made using the balance and free-flight techniques within the ranges $1 < Kn_\infty < 32$, $2.9 < M_\infty < 11.2$, $0.8 < T_w/T_\infty < 16.0$, and $2.5 < S_w < 3.2$. The balance data had less than ±1-percent scatter, but the free-flight data had as much as ±10-percent scatter. Drag measurements were made on two spheres which had different surface coatings, one painted black and the other gold, and any difference in the drag coefficients of the two spheres was less than the experimental error of the balance data.

It was found that the balance used was sensitive enough to measure the increase in drag on a 0.25-in.-diam sphere which was caused only by an increasing sphere wall temperature. Proper accounting of T_w in calculating $C_{D_{fm}}$ for normalizing C_D smoothed the drag data.

The sphere drag analysis provided a reasonable prediction of the drag coefficient throughout the transitional flow regime. It was in good agreement with the theory of

Willis, which appeared to be the most accurate of the three theories with which it was compared in the near free-molecular regime for the conditions considered. Furthermore, the present analysis was in good agreement with the experimental data for Knudsen numbers below which the previous theories were not valid.

REFERENCES

1. Engler, N. A. "Development of Methods to Determine Winds, Density, Pressure, and Temperature from the Robin Falling Balloon." University of Dayton Research Institute Report No. AF19(604)-7450, AFCRL-65-448, May 1965.

2. Baker, R.M.L., Jr. and Charwat, A. F. "Transitional Correction to the Drag of a Sphere in Free Molecule Flow." The Physics of Fluids, Vol. 1, No. 2, March-April, 1958, pp. 73-81.

3. Rose, M. H. "Drag on an Object in Nearly-Free Molecular Flow." The Physics of Fluids, Vol. 7, No. 8, August 1964, pp. 1262-1269.

4. Willis, D. R. "Methods of Analysis of Nearly Molecular Flow for a Satellite or Other Space Vehicle." (AD241900), General Electric Co., Space Sciences Labs, August 1960.

5. Kinslow, M. and Potter, J. L. "The Drag of Spheres in Rarefied Hypervelocity Flow." AEDC-TDR-62-205 (AD290519), December 1962.

6. Potter, J. L. and Miller,J. T. "Consideration of Simulation Parameters for Blunt Thick Bodies in Rarefied High-Speed Flows." AEDC-TR-68-242 (AD678159), November 1968.

7. Sims, W. H. "Experimental Sphere Drag Results in the Near-Free Molecule Regime." Rarefied Gas Dynamics, Vol. 1, Academic Press, New York, 1969, pp. 751-756.

8. Smolderen, J. J., Wendt, J. F., Naveau, J., and Bramlette, T. T. "Sphere and Cone Drag Coefficients in Hypersonic Transitional Flow." Rarefied Gas Dynamics, Vol. 1, Academic Press, New York, 1969, pp. 903-907.

9. Maslach, G. J., Willis, R. D., Tang, S., and Ko, D. "Recent Experimental and Theoretical Extensions of Nearly Free Molecular Flow." Rarefied Gas Dynamics, Vol. 1, Academic Press, New York, 1965, pp. 433-443.

10. Stephenson, W. B. and Whitfield, D. L. "Drag Measurements in a Low Density Gas Stream." AEDC-TR-70-25. (to be published).

11. Stephenson, W. B. "The Collection of a Normally Incident Low Density Supersonic Stream by a Cryogenic Surface." AEDC-TR-67-201 (AD663755), January 1968.

12. Whitfield, D. L. "Theoretical and Experimental Investigation of Boundary Layers in Low Density Hypersonic Axisymmetric Nozzles." AEDC-TR-68-193 (AD674597), September 1968.

13. Whitfield, D. L. and Lewis, C. H. "Analysis of Boundary Layers in Low Density Hypersonic Axisymmetric Nozzles, Including the Effects of Displacement, First-Order Transverse Curvature, Velocity Slip, and Temperature Jump." AIAA Paper 69-653, June 1969.

14. Potter, J. L. and Bailey, A. B. "Pressures in the Stagnation Regions of Blunt Bodies in the Viscous-Layer to Merged-Layer Regimes of Rarefied Flow." AEDC-TDR-63-168 (AD416004), September 1963.

15. Enkenhus, K. R. "Pressure Probes at Very Low Density." UTIA-R-43 (AD126534), January 1957.

16. White, R. B. "Hypersonic Viscous–Interaction and Rarefaction Effects on Impact Probes." AIAA Student Journal, Vol. 5, No. 2, April 1967, pp. 46-49.

17. Maslach, G. J. "Some Problems Associated with the Measurement of Very Low Pressures." AGARD Report 175, March 1958.

18. Rae, W. J. "Some Numerical Results on Viscous Low-Density Nozzle Flows in the Slender-Channel Approximation." AIAA Paper 69-654, June 1969.

19. Shidlovskii, V. P. Introduction to Dynamics of Rarefied Gases. American Elsevier Publishing Company, Inc., New York, 1967, pp. 32-33.

20. Perepukhov, V. A. "Aerodynamic Characteristics of a Sphere and Blunt-Nosed Cone in a Highly Rarefied Gas Flow." (Translated from Russian) FTD-MT-24-135-68 (AD681686), 1967.

APPENDIXES

I. ILLUSTRATIONS

II. TABLE

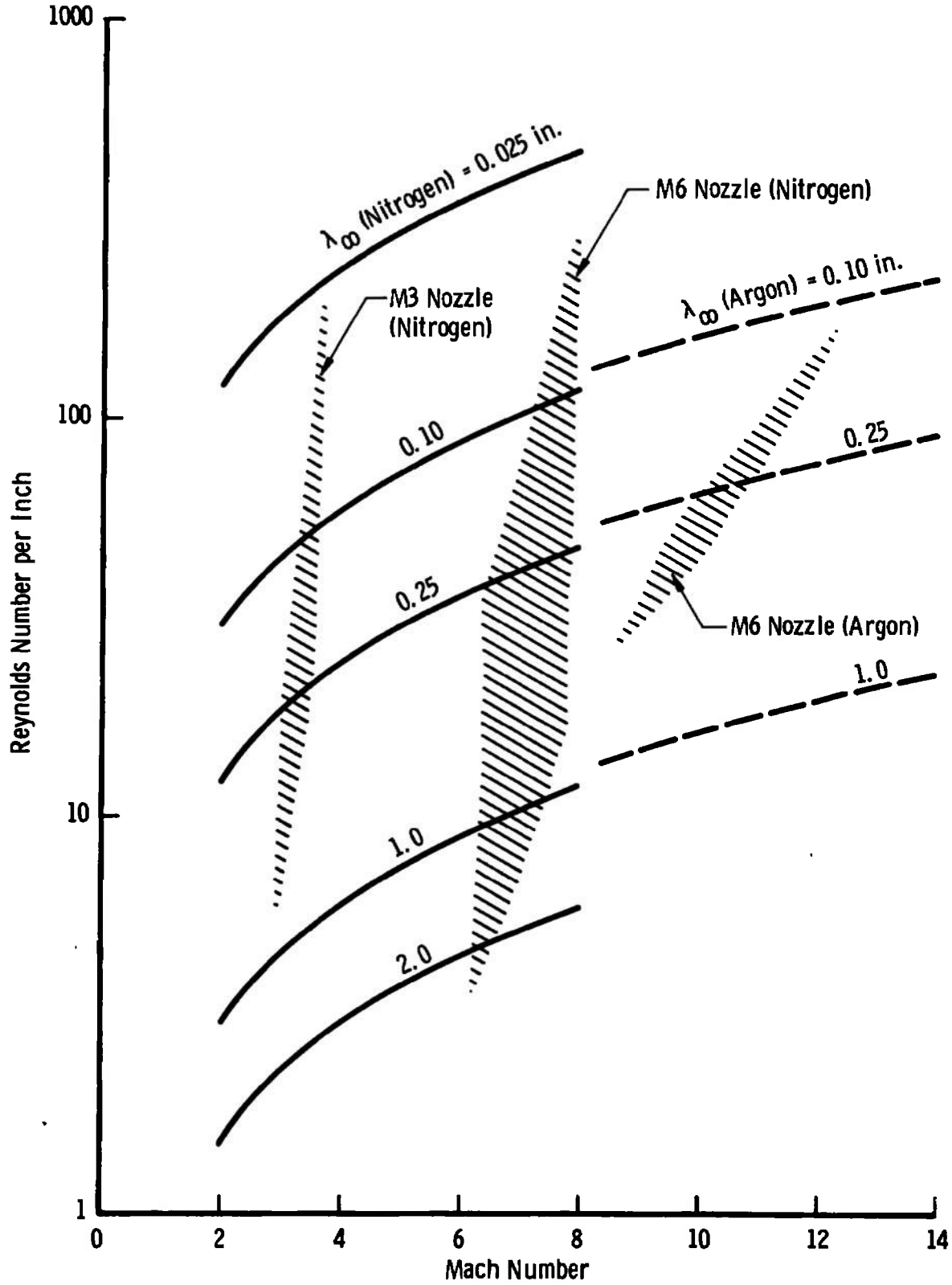

Fig. 1 Flow Conditions in the M3 and M6 Nozzles

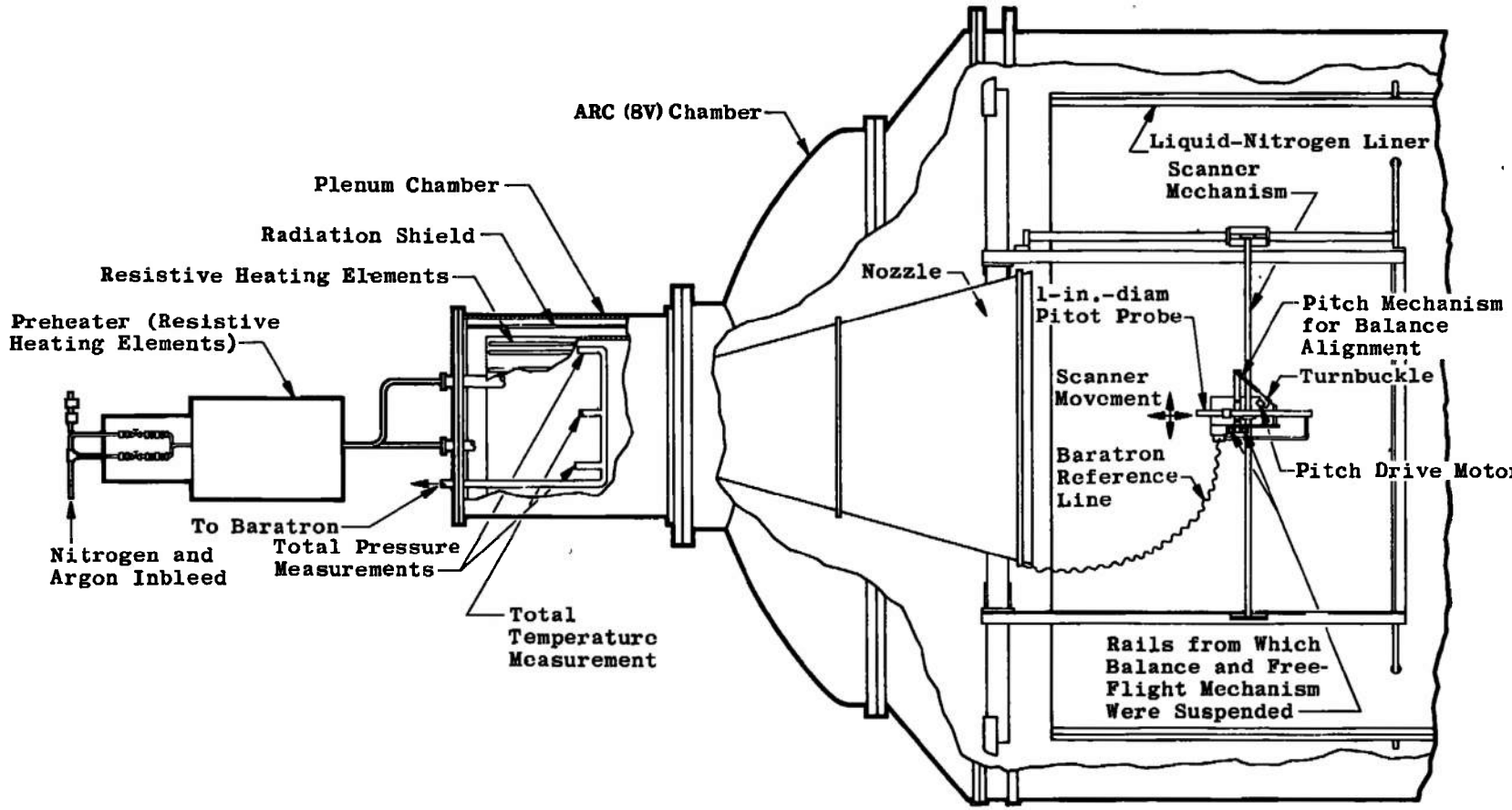

Fig. 2 Schematic of Low Density Tunnel, ARC (8V)

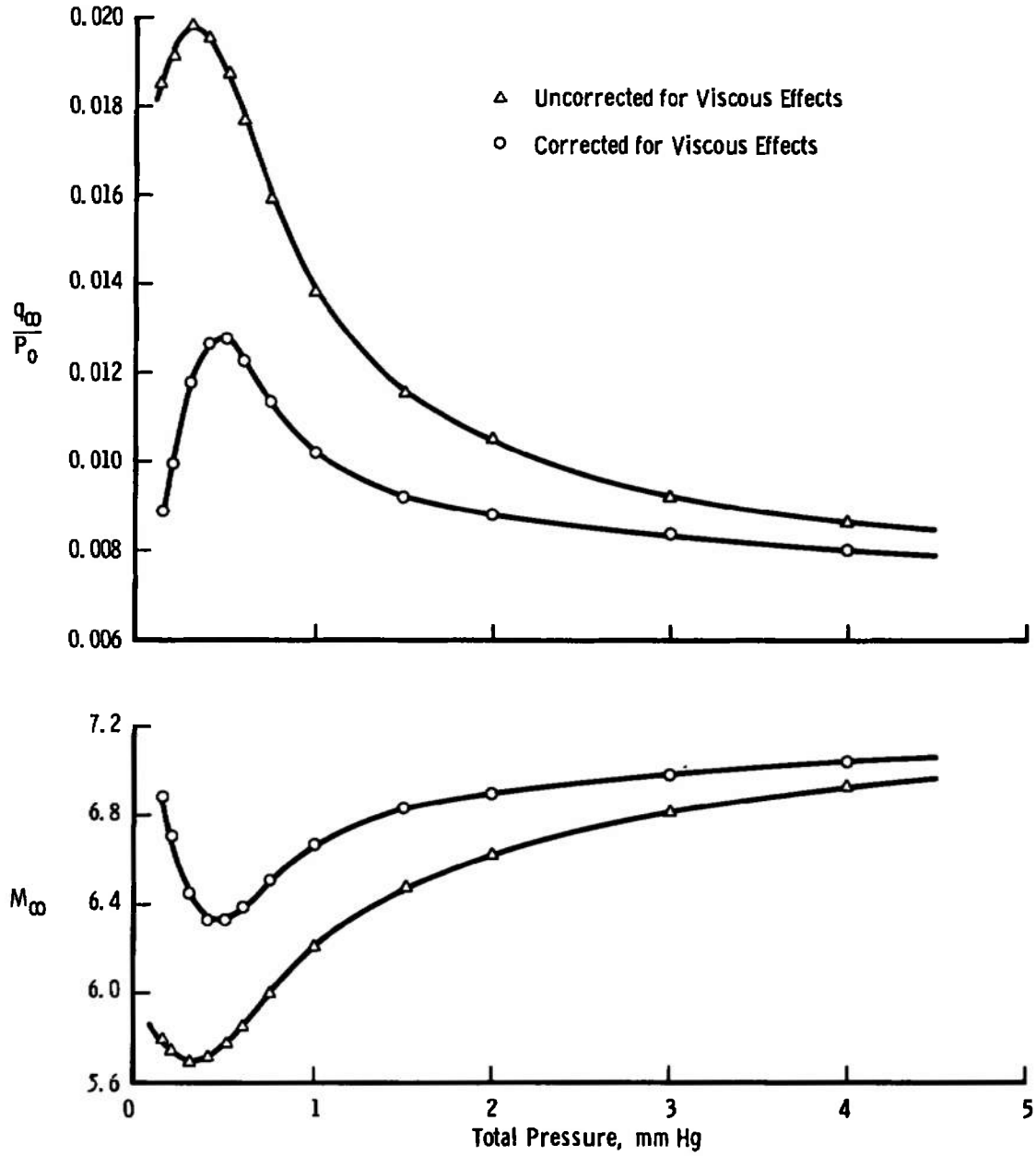

Fig. 3 Effect of Viscous Correction on Mach Number and Dynamic Pressure at the M6 Nozzle Exit

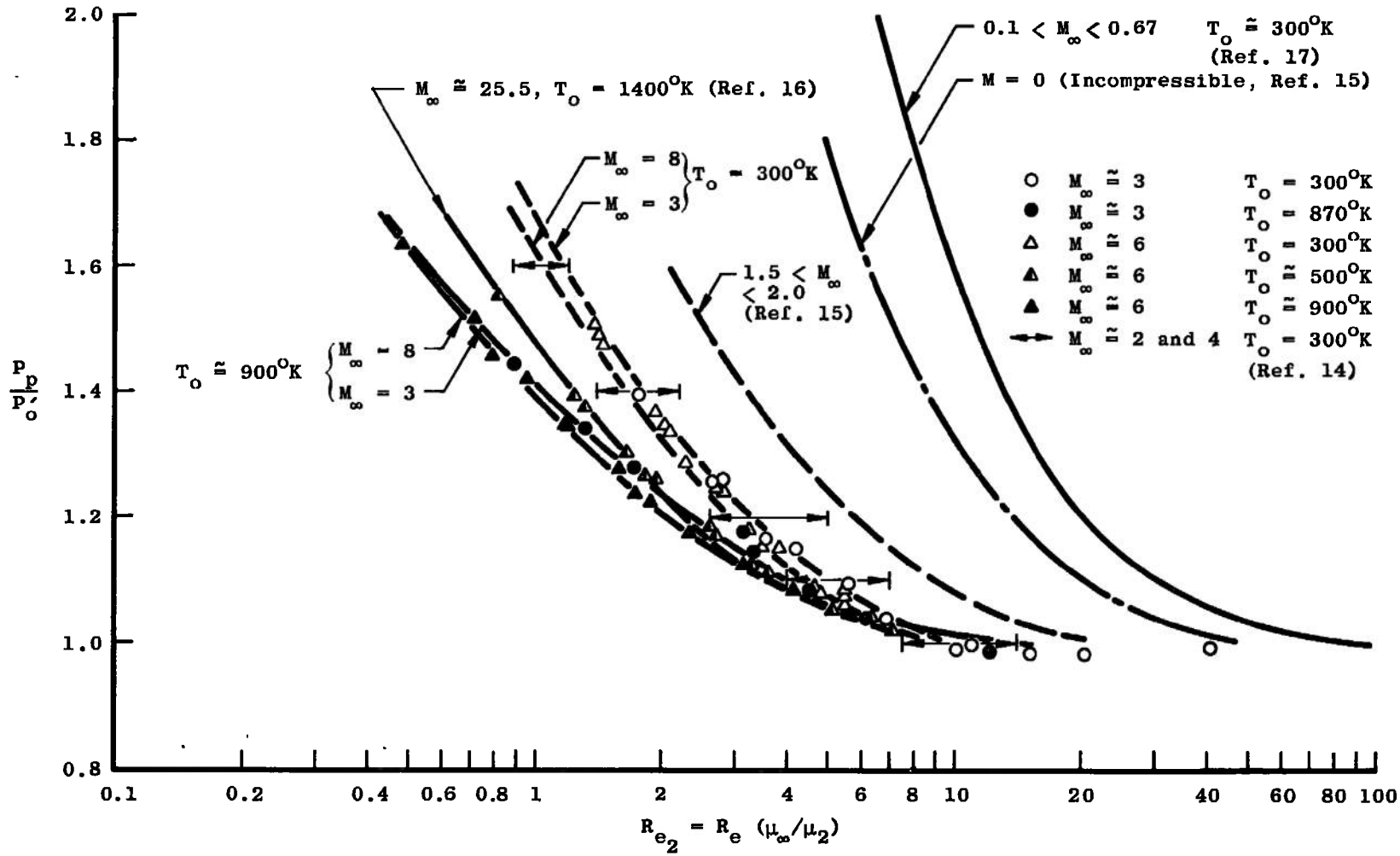

Fig. 4 Pitot Probe Viscous Correction Data

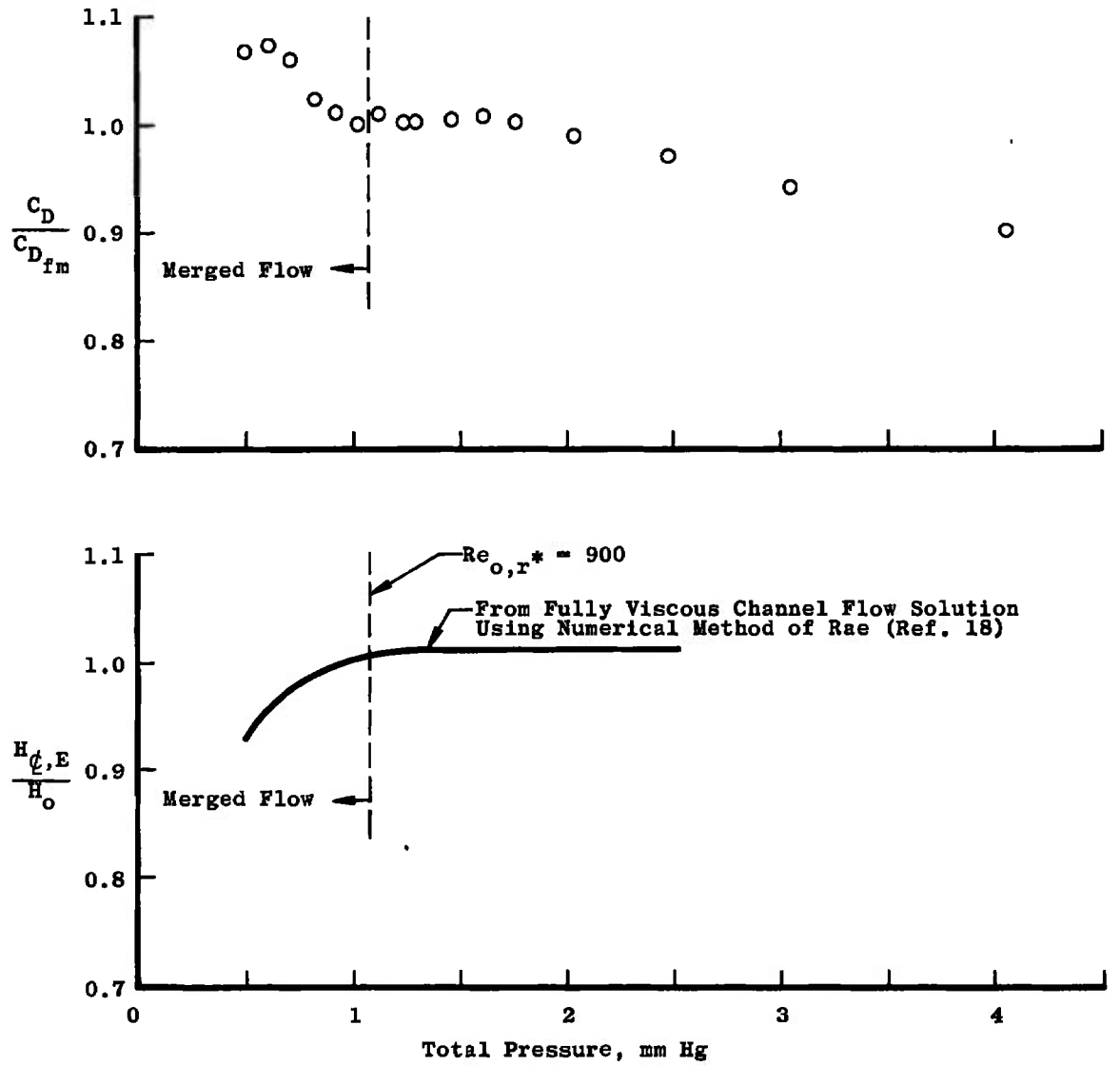

Fig. 5 Increase in $C_D/C_{D_{fm}}$ and Decrease in $H_{\mathcal{L}}/H_o$ for the M6 Nozzle (T_o = 800°K)

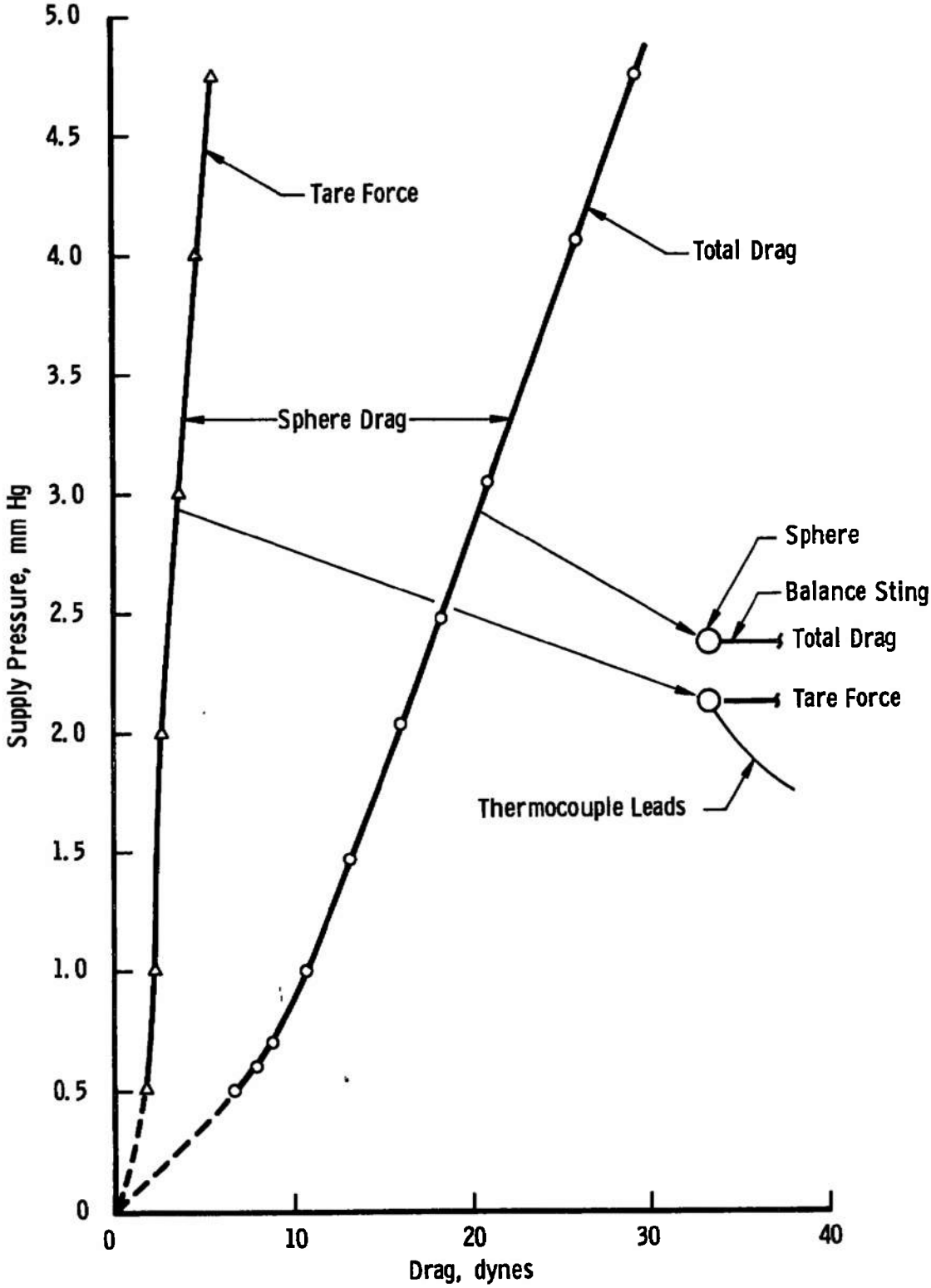

Fig. 6 Tare Force and Total Drag Measurements Using 0.25-in.-diam Sphere on Drag Balance in M6 Nozzle Flow

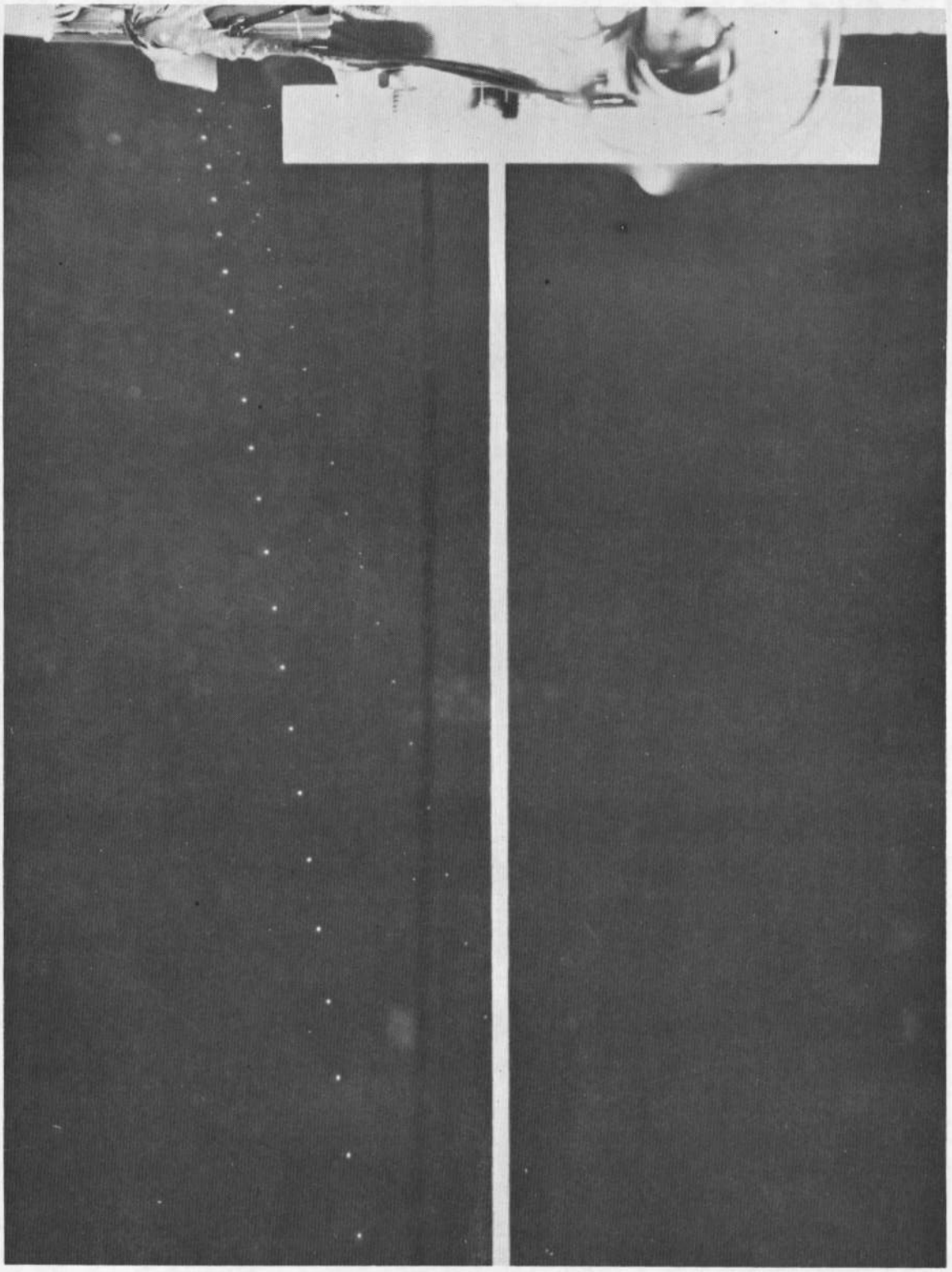

Fig. 7 Falling Spheres Using the Free-Flight Technique

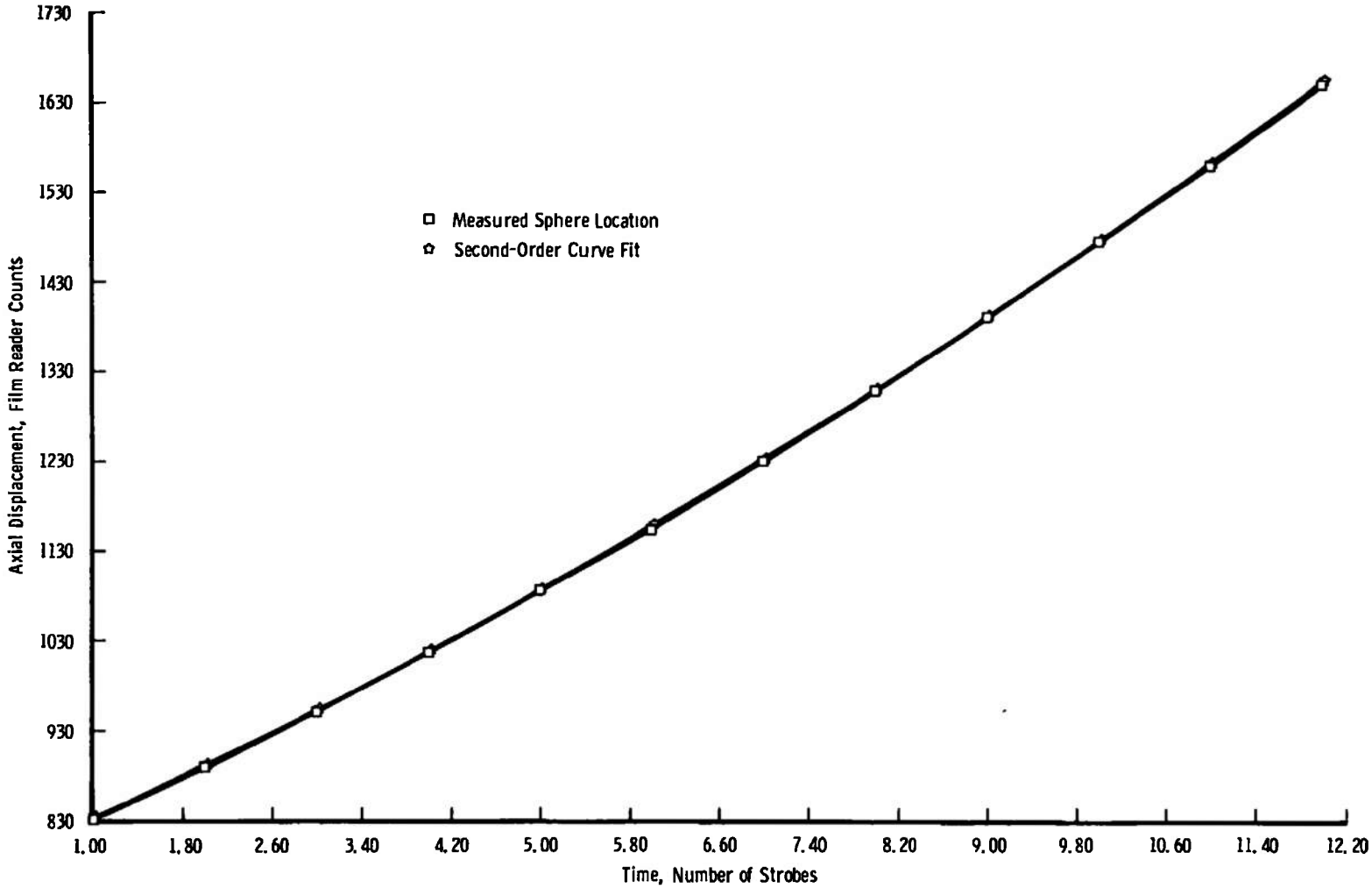

Fig. 8 Curve Fit of the Axial Displacement of a Sphere versus Time

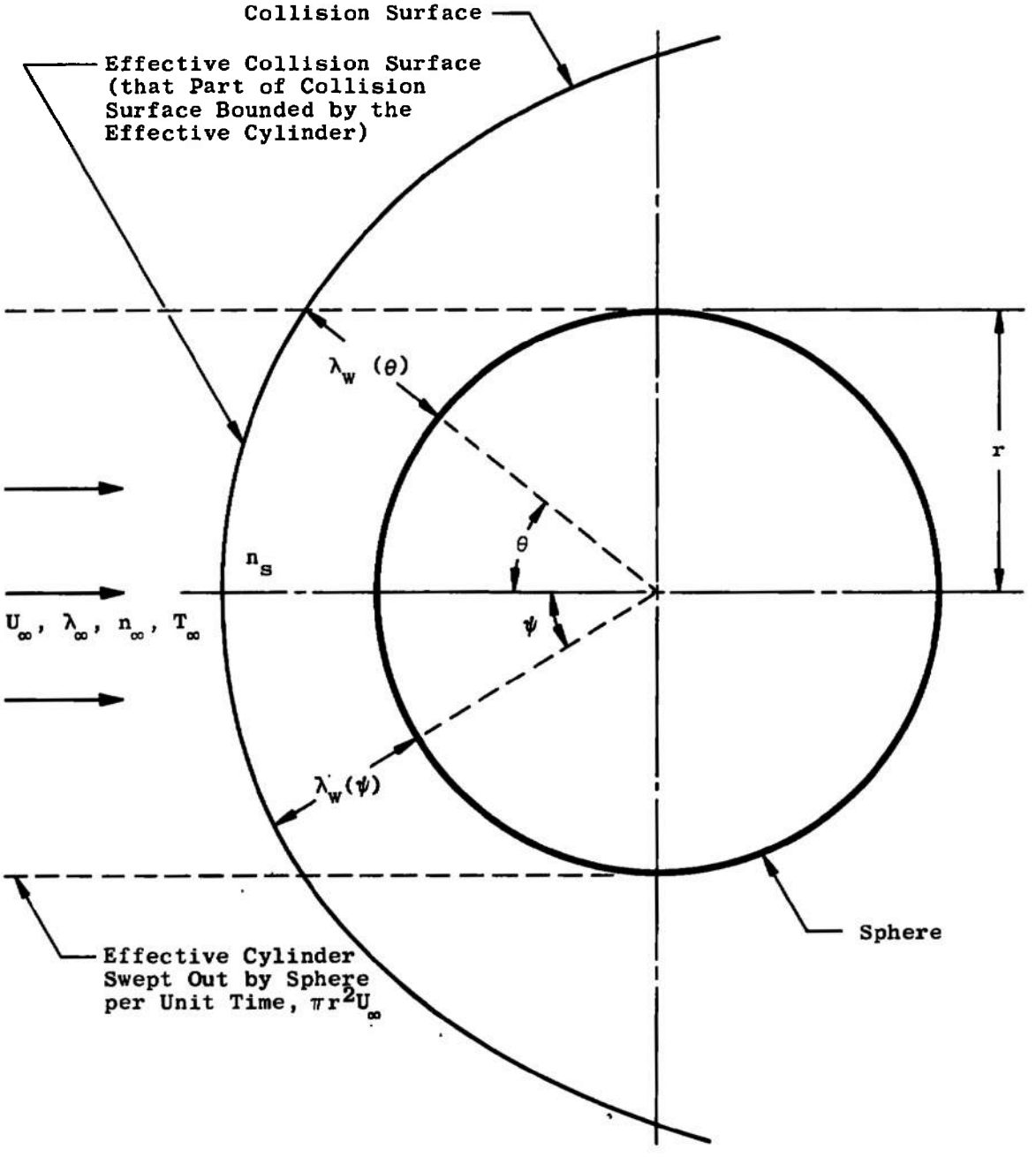

Fig. 9 Assumed Model of the Rarefied Flow about a Sphere

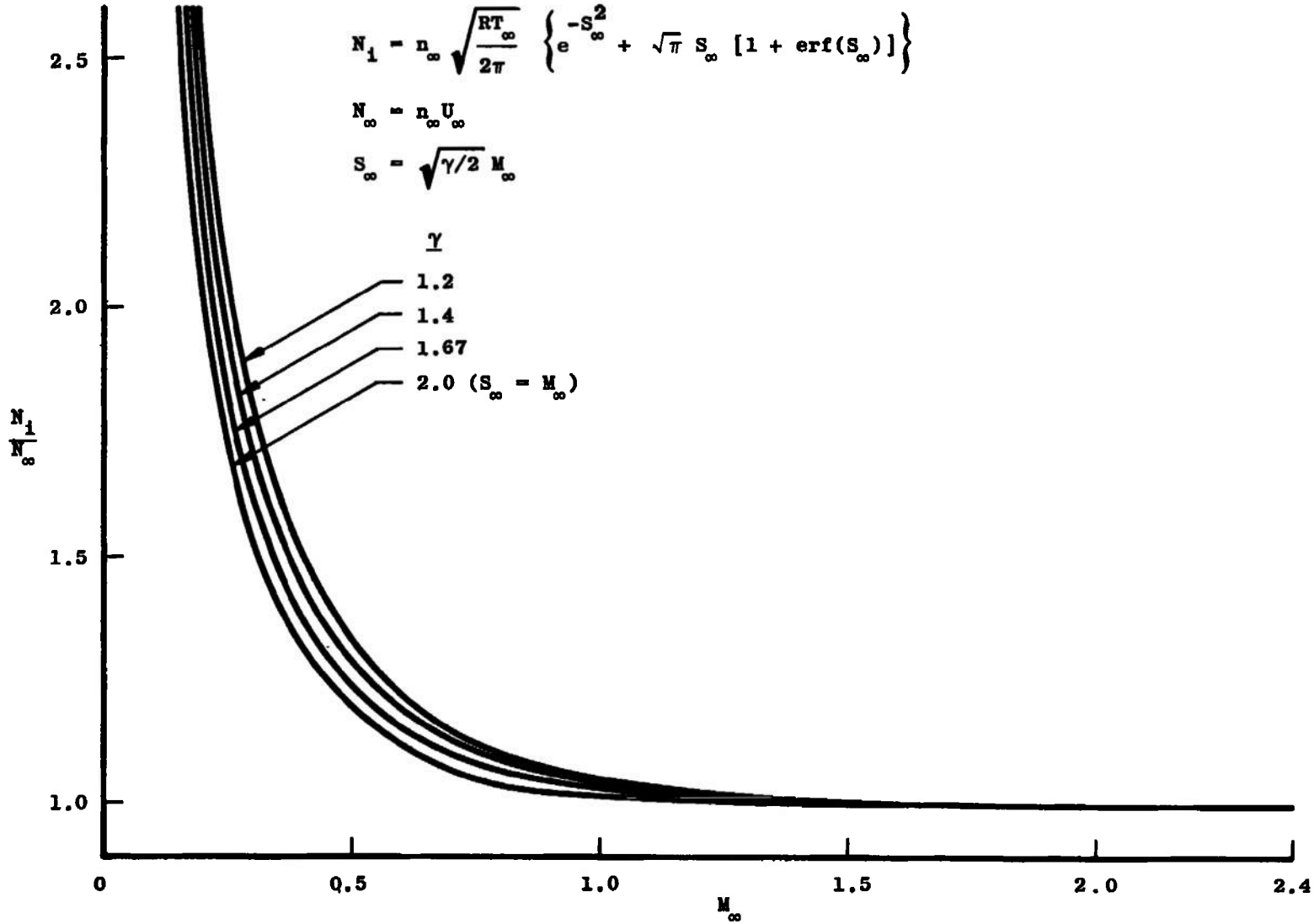

Fig. 10 Incident Flux of Molecules on a Sphere in Free-Molecular Flow

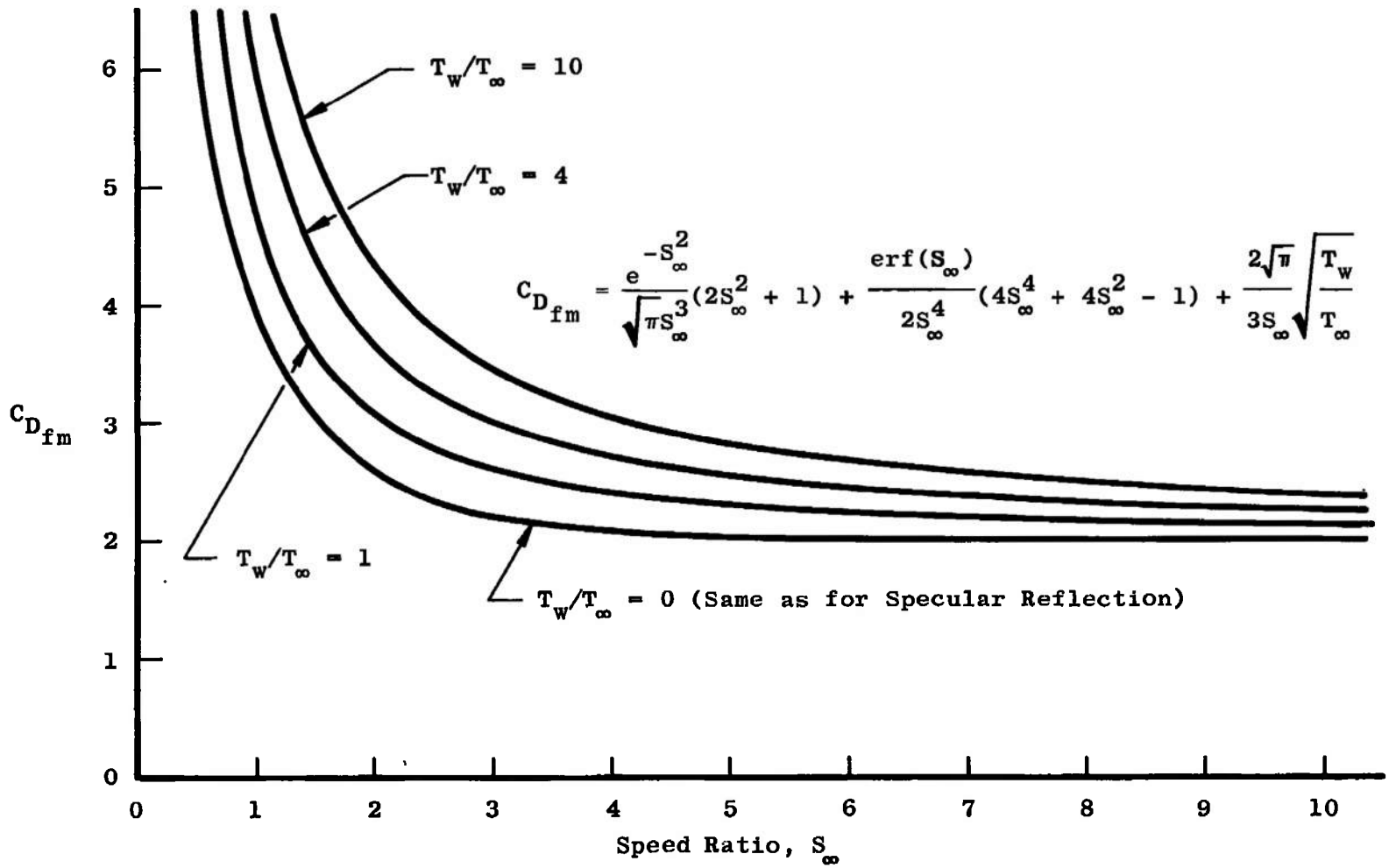

Fig. 11 Free-Molecular Sphere Drag Coefficients for Diffuse Reflection and Complete Accommodation

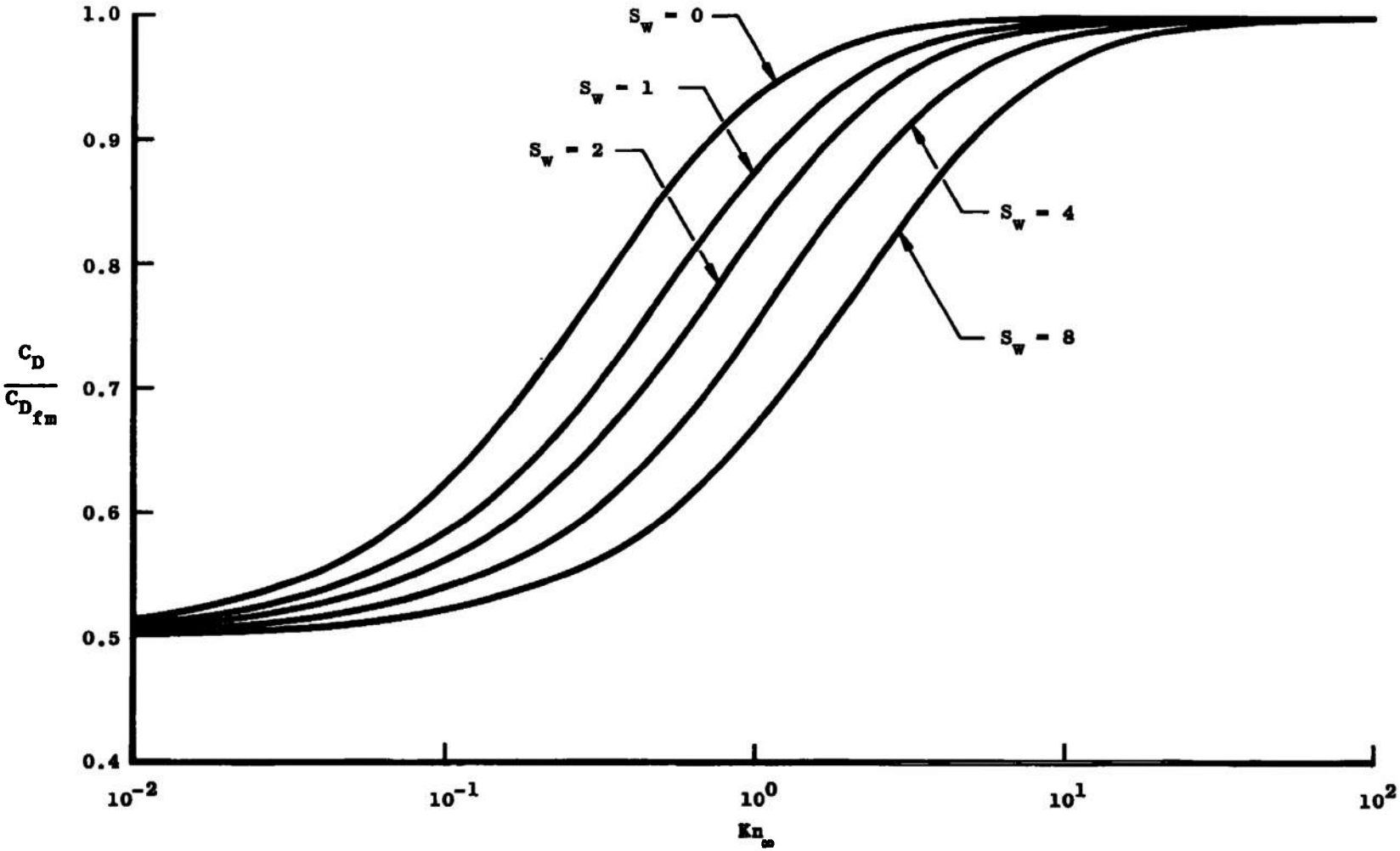

Fig. 12 Sphere Drag Coefficients in the Transitional Flow Regime According to Eqs. (19) and (20)

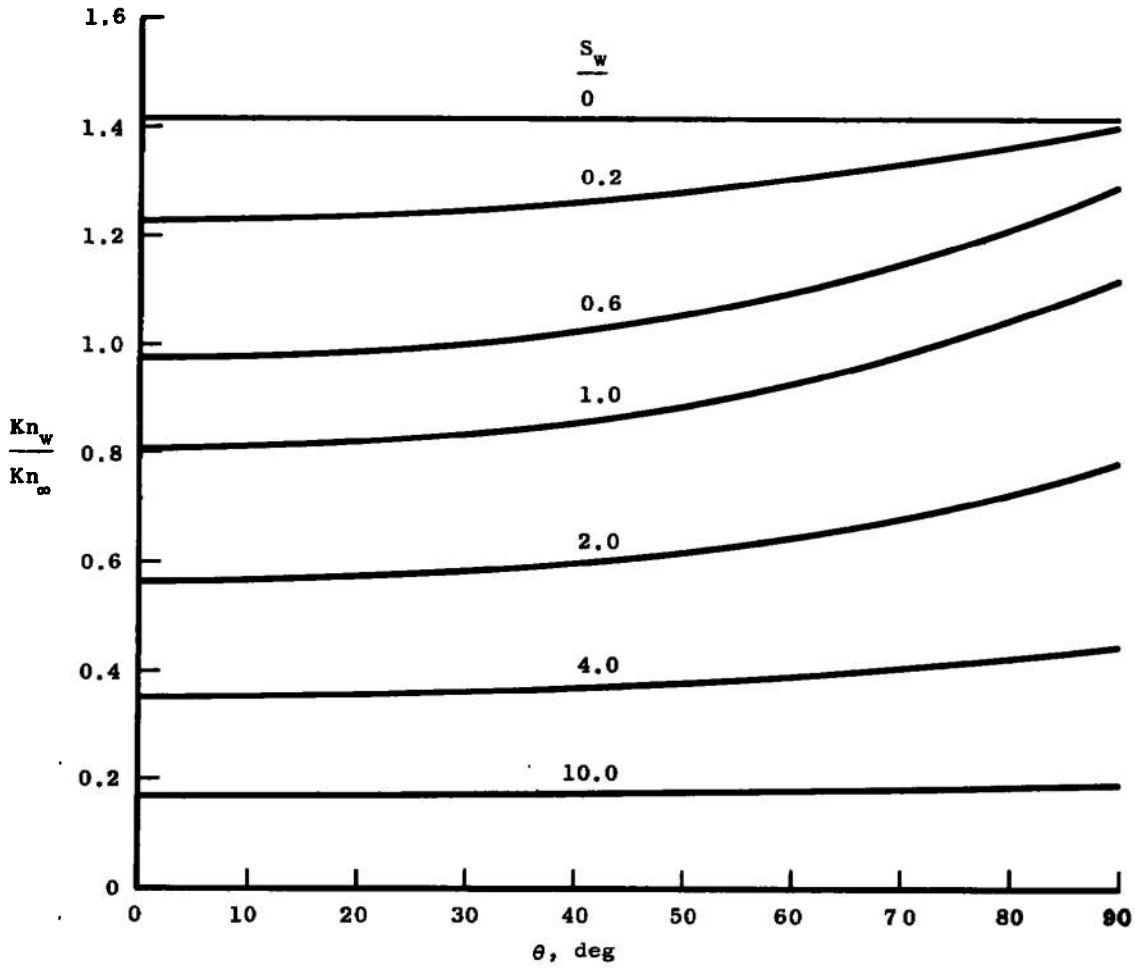

Fig. 13 Effect of θ on Kn_w/Kn_∞

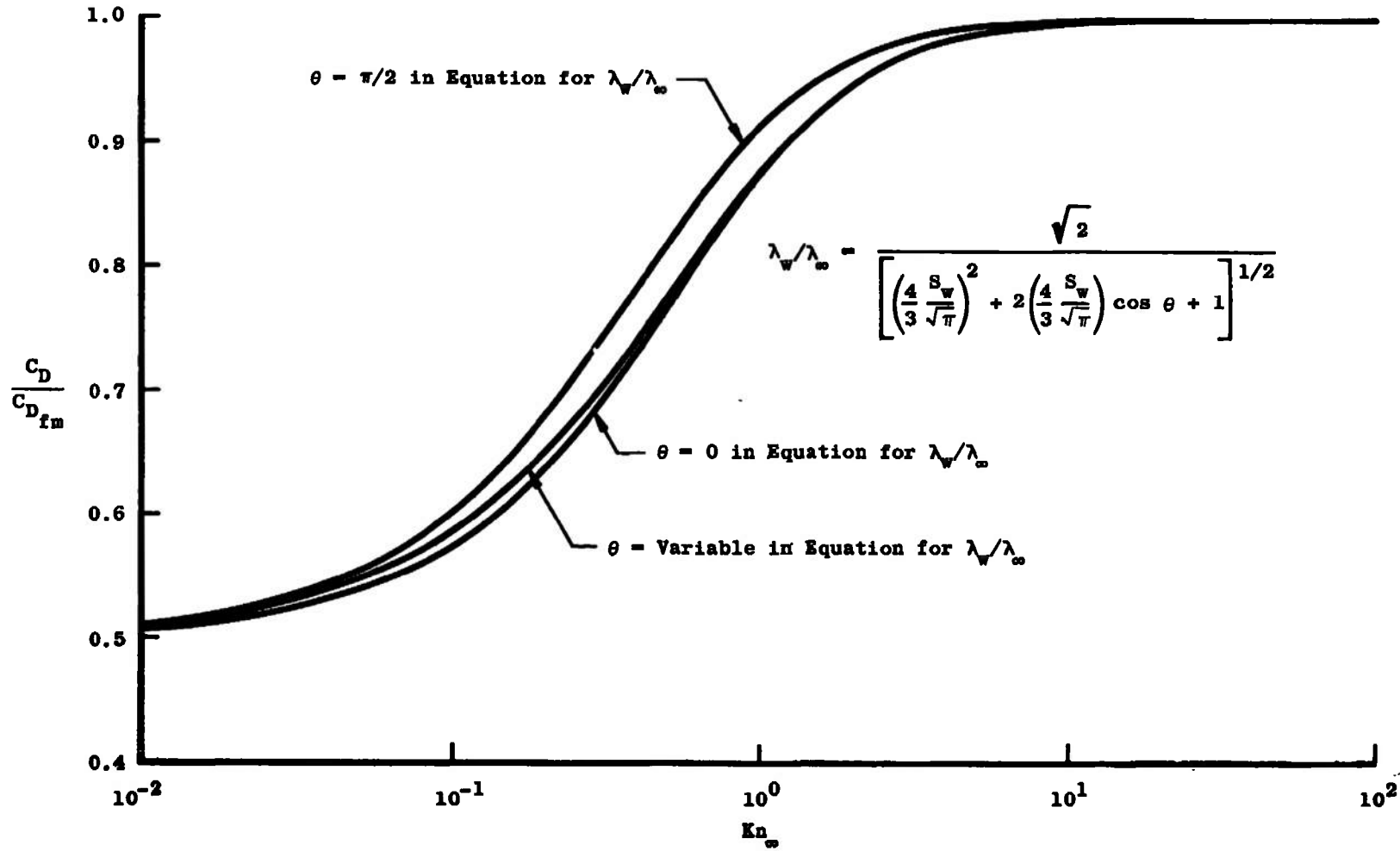

Fig. 14 Sphere Drag Coefficients for Constant and Variable λ_w with $S_w = 1$

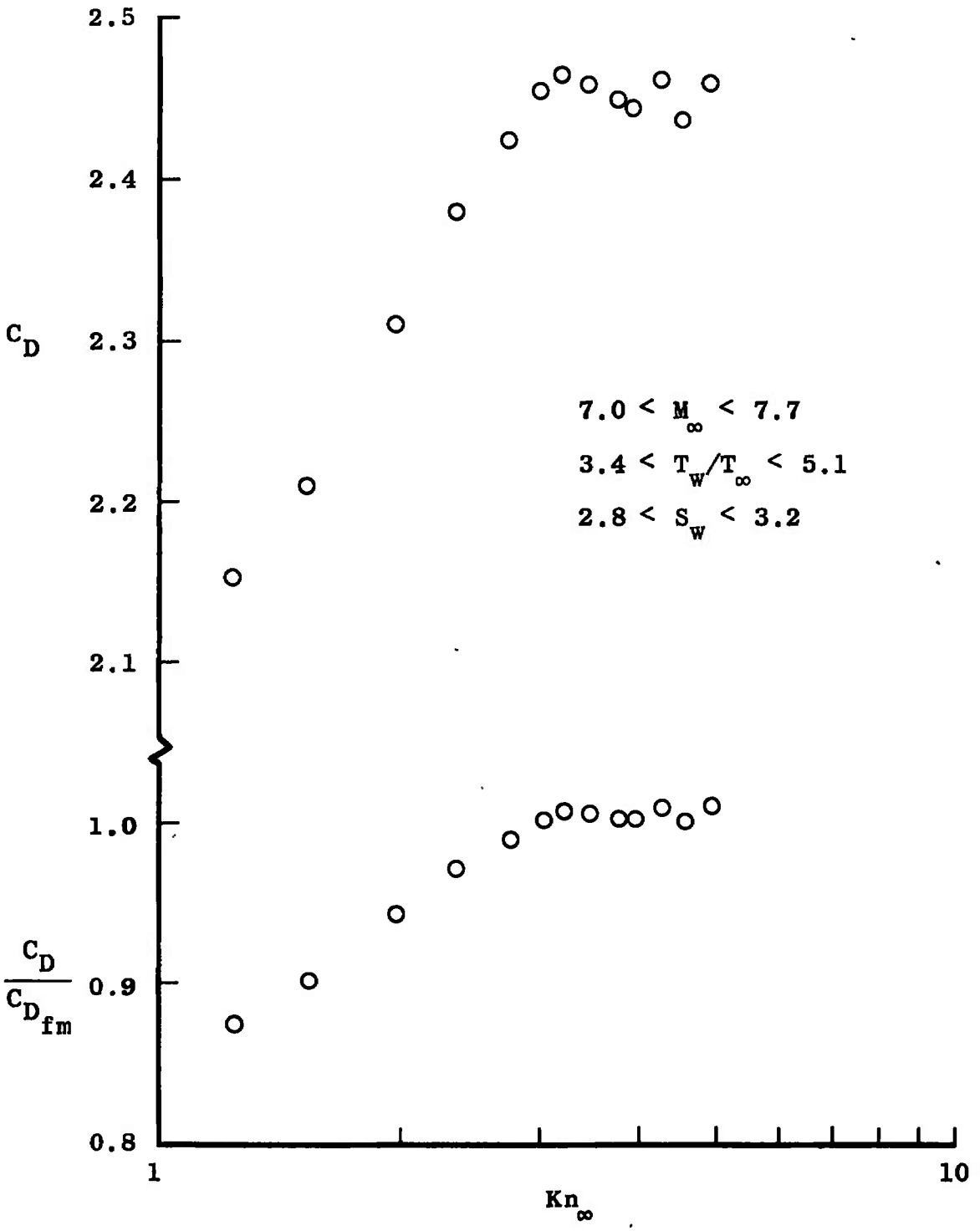

Fig. 15 Effect of Normalizing C_D by $C_{D_{fm}}$

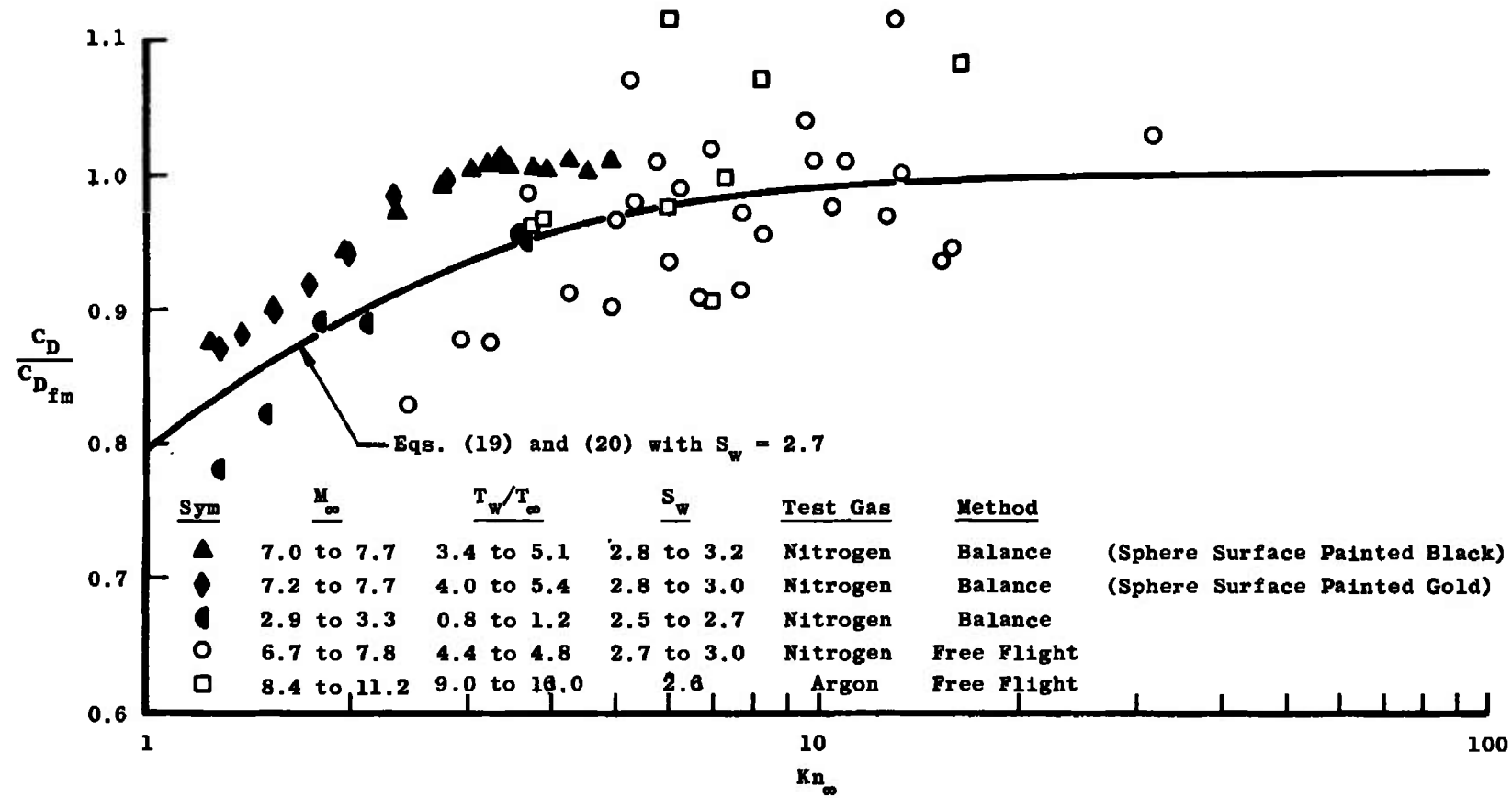

Fig. 16 Balance and Free-Flight Sphere Drag Data with Analytical Results

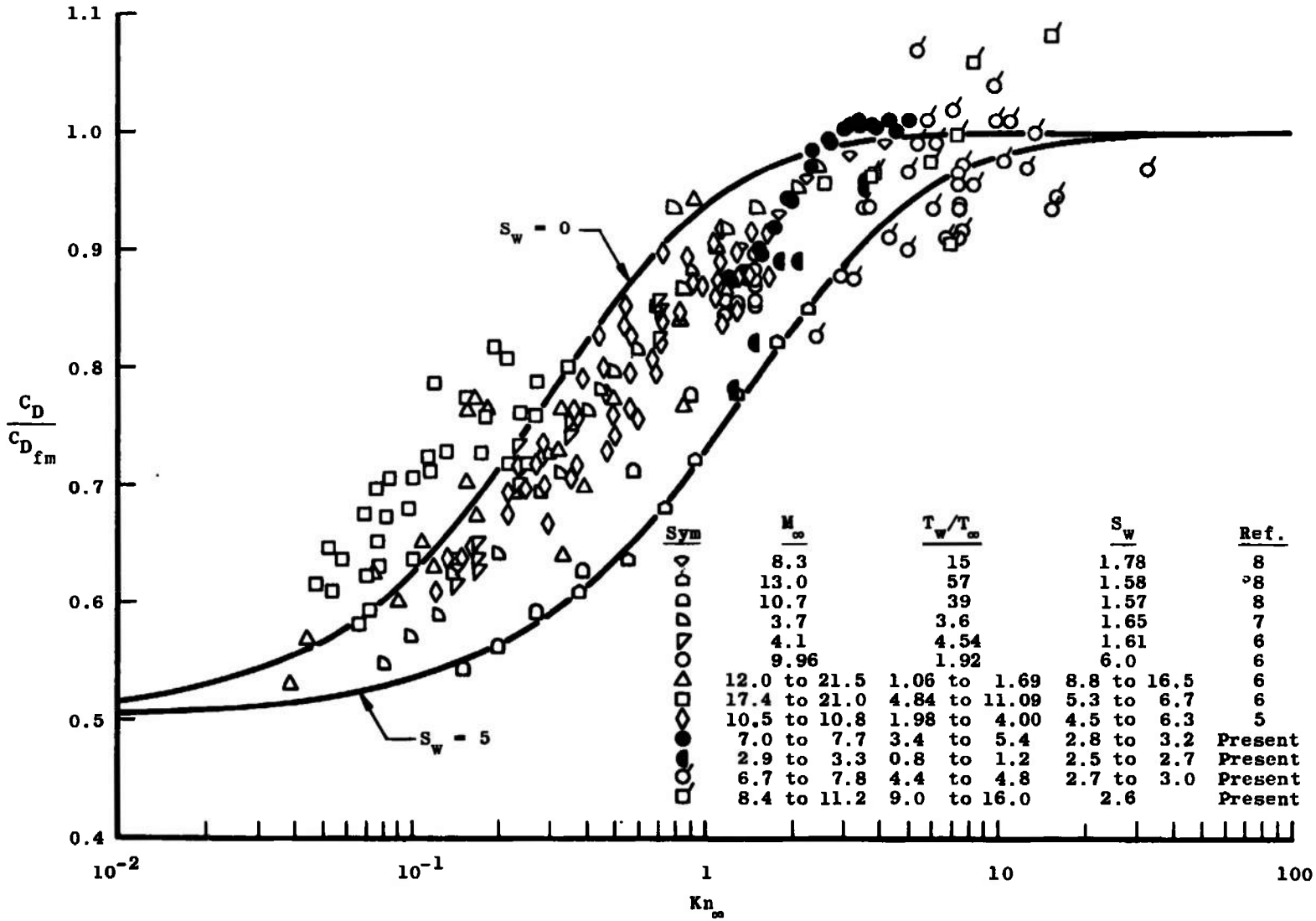

Fig. 17 Trend of Analytical Results and Experimental Data in the Transitional Flow Regime

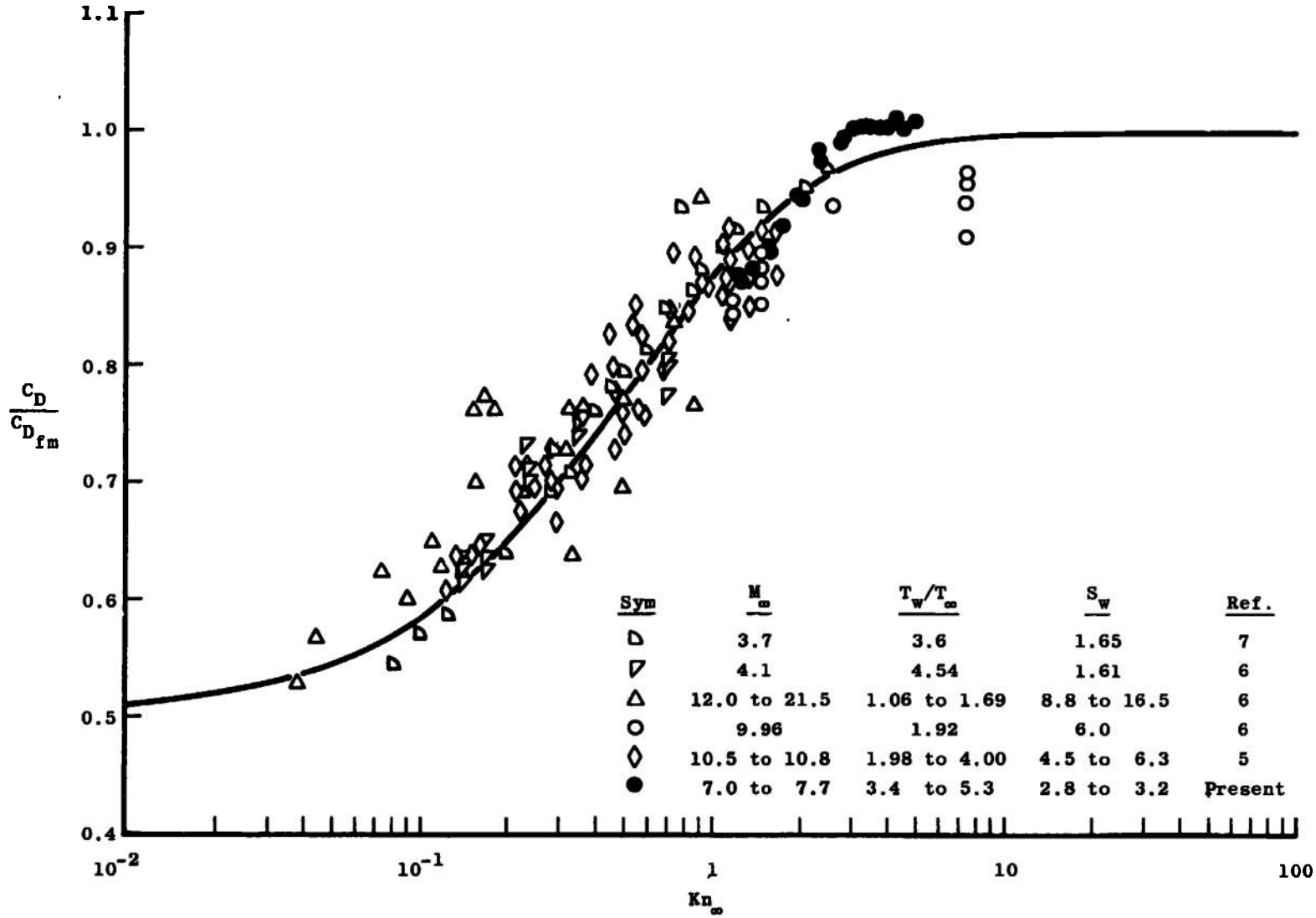

Fig. 18 Analytical Result with S_w = 1 and Some Experimental Data with Little Scatter

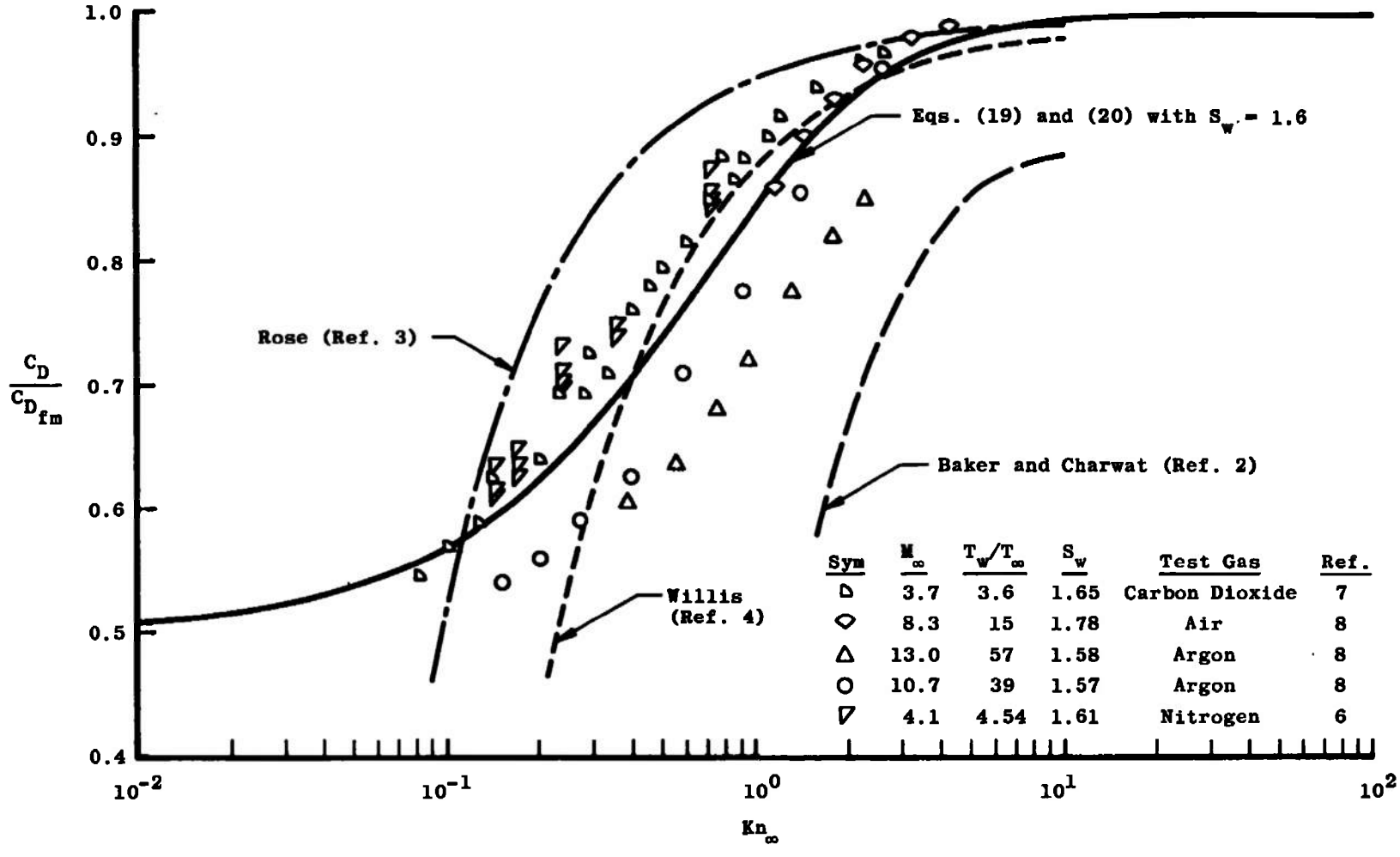

Fig. 19 Comparison of Eq. (19) with Other Theories and Available Experimental Data for S_w near 1.6

TABLE I
SPHERE DRAG COEFFICIENTS AND FLOW CONDITIONS
a. Balance Data

M_∞	Re_∞	Kn_∞	T_w/T_∞	S_w	C_D	$C_D/C_{D\,fm}$	Test Gas
6.98	2.12	4.92	3.40	3.16	2.460	1.012	Nitrogen
7.02	2.30	4.55	3.49	3.14	2.437	1.001	
7.06	2.47	4.26	3.58	3.12	2.462	1.011	
7.10	2.68	3.95	3.68	3.09	2.445	1.003	
7.13	2.82	3.77	3.77	3.07	2.450	1.003	
7.19	3.10	3.45	3.89	3.05	2.460	1.006	
7.25	3.37	3.21	4.01	3.03	2.465	1.008	
7.31	3.59	3.03	4.15	3.00	2.455	1.003	
7.41	4.01	2.75	4.34	2.97	2.425	0.990	
7.49	4.75	2.35	4.51	2.95	2.380	0.972	
7.57	5.72	1.97	4.67	2.93	2.310	0.942	
7.65	7.40	1.54	4.87	2.90	2.210	0.901	
7.70	9.25	1.24	5.05	2.86	2.152	0.875	
7.22	3.20	3.36	4.08	2.99	2.480	1.012	
7.40	3.95	2.79	4.43	2.94	2.437	0.993	
7.50	4.81	2.32	4.70	2.89	2.418	0.984	
7.57	5.70	1.98	4.86	2.87	2.315	0.942	
7.61	6.51	1.74	5.00	2.85	2.265	0.919	
7.65	7.36	1.55	5.13	2.82	2.220	0.900	
7.68	8.30	1.38	5.25	2.80	2.172	0.880	
7.70	9.03	1.27	5.37	2.78	2.156	0.871	
2.90	1.19	3.65	0.80	2.71	2.615	0.951	
2.92	1.23	3.55	0.85	2.65	2.630	0.955	
3.07	2.16	2.12	0.90	2.71	2.405	0.890	
3.19	2.64	1.80	1.00	2.67	2.420	0.890	
3.28	3.23	1.51	1.10	2.61	2.250	0.820	
3.34	3.89	1.28	1.20	2.55	2.140	0.778	

TABLE I (Concluded)
b. Free-Flight Data

M_∞	Re_∞	Kn_∞	T_w/T_∞	S_w	C_D	$C_D/C_{D\,fm}$	Test Gas
7.65	4.63	2.46	4.69	2.95	2.010	0.828	Nitrogen
7.69	2.28	5.02	4.73	2.96	2.340	0.966	
7.79	1.11	10.5	4.85	2.96	2.352	0.976	
7.59	2.10	5.37	4.62	2.95	2.379	0.979	
7.69	1.04	11.00	4.73	2.96	2.447	1.011	
7.50	3.82	2.92	4.52	2.95	2.162	0.878	
7.53	1.88	5.99	4.55	2.95	2.300	0.934	
7.45	3.40	3.27	4.47	2.95	2.153	0.875	
7.47	1.67	6.66	4.49	2.95	2.237	0.908	
7.51	0.83	13.40	4.53	2.95	2.440	1.000	
7.51	0.85	13.20	4.53	2.95	2.750	1.118	
7.37	3.00	3.66	4.38	2.94	2.412	0.986	
7.45	1.45	7.64	4.47	2.95	2.507	0.913	
7.29	2.55	4.26	4.29	2.94	2.228	0.911	
7.23	1.30	8.31	4.23	2.94	2.341	0.956	
7.15	2.14	4.97	4.14	2.94	2.203	0.899	
7.11	1.08	9.82	4.10	2.94	2.480	1.010	
7.02	0.83	12.65	4.01	2.93	2.390	0.969	
6.71	0.63	15.80	3.69	2.92	2.337	0.946	
6.69	0.65	15.43	3.67	2.92	2.310	0.935	
6.78	0.32	31.50	3.76	2.92	2.532	1.029	
7.32	1.14	9.54	4.47	2.89	2.542	1.040	
7.48	1.45	7.68	4.65	2.90	2.385	0.971	
7.58	1.63	6.95	4.77	2.90	2.500	1.020	
7.65	1.84	6.22	4.85	2.90	2.397	0.990	
7.72	2.00	5.74	4.93	2.91	2.440	1.009	
7.76	2.22	5.22	4.97	2.91	2.623	1.070	
8.41	1.67	8.23	8.52	2.63	2.664	1.071	Argon
8.42	0.84	16.3	8.52	2.63	2.700	1.083	
9.42	2.20	6.96	11.17	2.61	2.257	0.905	
9.52	2.24	7.26	11.29	2.59	2.482	0.998	
10.04	2.73	6.00	12.60	2.59	2.772	1.117	
10.06	2.74	5.98	12.68	2.58	2.427	0.977	
11.12	4.67	3.88	15.38	2.59	2.395	0.967	
11.14	4.87	3.73	15.50	2.59	2.380	0.962	

UNCLASSIFIED

Security Classification

DOCUMENT CONTROL DATA - R & D

(Security classification of title, body of abstract and indexing annotation must be entered when the overall report is classified)

1. ORIGINATING ACTIVITY *(Corporate author)* Arnold Engineering Development Center, ARO, Inc., Operating Contractor, Arnold Air Force Station, Tennessee 37389	2a. REPORT SECURITY CLASSIFICATION UNCLASSIFIED 2b. GROUP N/A

3. REPORT TITLE

SPHERE DRAG IN THE FREE-MOLECULAR AND TRANSITIONAL FLOW REGIMES

4. DESCRIPTIVE NOTES *(Type of report and inclusive dates)*

Final Report - April 14 to September 26, 1969

5. AUTHOR(S) *(First name, middle initial, last name)*

David L. Whitfield and William B. Stephenson, ARO, Inc.

6. REPORT DATE	7a. TOTAL NO. OF PAGES	7b. NO. OF REFS
April 1970	43	20

8a. CONTRACT OR GRANT NO.	9a. ORIGINATOR'S REPORT NUMBER(S)
F40600-69-C-0001	
b. PROJECT NO. 6690	AEDC-TR-70-32
c. Program Element 62101F	9b. OTHER REPORT NO(S) *(Any other numbers that may be assigned this report)*
d. Task 669002	N/A

10. DISTRIBUTION STATEMENT

This document has been approved for public release and sale; its distribution is unlimited.

11. SUPPLEMENTARY NOTES	12. SPONSORING MILITARY ACTIVITY
Available in DDC	Air Force Cambridge Research Laboratory (CRMP), L.G. Hanscom Field, Bedford, Mass. 01730

13. ABSTRACT

Results are presented of sphere drag measurements made in the free-molecular and transitional flow regimes. The drag data were obtained using a drag balance and the free-flight technique. Conditions for which measurements were made are within the ranges $1 < Kn_\infty < 32$, $2.9 < M_\infty < 11.2$, $0.8 < T_W/T_\infty < 16.0$, and $2.5 < S_W < 3.2$. An analysis of the drag on a sphere in rarefied flow is also presented, and the results are compared with experimental data and other theories. The analytical results well predict the trend of the experimental data in the transition regime and remain valid at Knudsen numbers for which previous theories are not applicable.

DD FORM 1 NOV 68 1473

UNCLASSIFIED

Security Classification

14. KEY WORDS	LINK A		LINK B		LINK C	
	ROLE	WT	ROLE	WT	ROLE	WT
aerodynamic drag						
weight indicators						
free molecule flow						
transition flow						
2 Knudsen flow						
free flight trajectories						
rarefied gas dynamics						

1. Sphere -- drag

1 - 2.

AFSC
Arnold AFS Tenn